

学位論文（要約）

Interface electronic and magnetic structures in atomic-scale
Mn/Fe heterostructures

(原子スケール Mn/Fe ヘテロ構造における
界面電子磁気構造)

平成29年12月博士(理学)申請

東京大学大学院理学系研究科
物理学専攻

中島 脩平

Dissertation

**Interface electronic and magnetic structures in
atomic-scale Mn/Fe heterostructures**

A thesis submitted for the degree of Doctor of Science

Shuhei Nakashima

Department of Physics, Graduate School of Science
The University of Tokyo

December, 2017

Abstract

The objective of this thesis is to connect atomic scale interfacial structural characterization to electronic and magnetic properties of Mn/Fe thin film heterostructures using spin-polarized scanning tunneling microscopy/spectroscopy (SP-STM/STS) and X-ray absorption spectroscopy/magnetic circular dichroism (XAS/XMCD).

We first identify the growth of the Mn thin films grown on fcc-Fe/Cu(001) surface studied by STM/STS. Thickness dependent STM/STS measurements reveal the changes of the structural and electronic properties due to the intermixing between Mn and Fe thin films at the interface. Mn films thicker than five ML reveal that reconstructed pure Mn layer starts to grow with the same electronic structure and geometrically equivalent interlayer spacings. Second, we show a dominant interfacial factor characterizing electronic and magnetic properties of the entire system dynamically changes with the amount of the Mn overlayer combining XAS/XMCD with STM/STS. Element specific magnetization curves of the Fe layer exhibit a spin reorientation transition from out-of-plane to in-plane direction with increasing Mn thickness. Corresponding atomic-scale characterizations of structural and electronic properties successfully unravel the roles of entangled interfacial factors, and clarify the driving force of transition. Finally, the surface magnetic ordering in Mn/Fe thin film heterostructure is studied by SP-STM/STS. Spin-averaged and spin-polarized STS reveal a spin-polarized state around the Fermi level E_F . Spin resolved differential conductance exhibits magnetic contrasts due to the magnetic exchange interaction between Mn and Fe thin film. Analysis of the intensity of the differential conductance signal reveals the Mn magnetic domain structure reflecting the underlying Fe magnetic domain structure and interfacial magnetic anisotropy.

Contents

1	Introduction	1
1.1	Preface	1
1.2	Purpose	3
1.3	Outline	4
2	Experimental and theoretical background	5
2.1	Scanning tunneling microscopy and spectroscopy	5
2.1.1	History and concept	5
2.1.2	Topography	6
2.1.3	Spectroscopy	8
2.1.4	Spin polarized STM	9
2.2	X-ray absorption spectroscopy	12
2.3	X-ray magnetic circular dichroism	13
3	Instrumentation and Preparation	15
3.1	The ultra-high vacuum systems	15
3.1.1	Setup for scanning tunneling microscope	16
3.1.2	Setup for X-ray absorption spectroscopy	17
3.2	Sample preparation	18
3.2.1	Substrate preparation	18
3.2.1.1	Cleaning the Cu(001) surface	18
3.2.1.2	Deposition of the Fe and Mn	19
3.2.2	Tip preparation	22
3.2.2.1	Soft indentation (dipping of the tip)	24
3.2.2.2	Preparation of magnetic tips	25

CONTENTS

4	Growth and Magnetism of Fe/Cu(001)	27
4.1	Introduction	27
4.2	Structural and Magnetic properties of Fe thin films on Cu(001) – a Literature review	27
4.3	Experiments on Fe/Cu(001)	30
4.3.1	Topography and structure of Fe thin films on Cu(001)	30
4.3.2	Magnetic properties of Fe thin films on Cu(100)	31
4.4	Conclusion	34
5	Growth of Mn/fcc-Fe(001)	37
5.1	Introduction	37
5.2	Growth and structure of Mn thin films on fcc-Fe/Cu(001)	38
5.2.1	Preparation of the Cu(001) and Fe/Cu(001) surfaces	38
5.2.2	Growth of Mn thin films on fcc-Fe/Cu(001)	40
5.2.3	Surface atomical structure	45
5.3	Conclusion	46
6	Dynamic interface formation in magnetic thin film heterostructures	49
6.1	Introduction	50
6.2	Magnetic anisotropy of buried interface	51
6.2.1	Spin reorientation in fcc Fe thin films	51
6.2.2	Mn thickness dependence of the Fe magnetization	53
6.3	Interfacial structure changes	55
6.3.1	Interfacial alloy formation with atomic-scale	55
6.3.2	Interfacial electronic structure	61
6.3.3	Spin- and orbital- resolved LDOS of fcc Fe thin films on Cu(001) explained by first-principles calculations	63
6.4	Conclusion	65
7	Observation of the surface and interface magnetism in Mn/Fe heterostructure	67
7.1	Introduction	68
7.2	Structure, growth, magnetic anisotropy	68

CONTENTS

7.3	Spin-resolved measurements	70
7.3.1	Comparing non spin-polarized and spin-polarized tip	70
7.3.2	Control of the tip magnetization directions	74
7.3.3	Domain structure and domain wall	77
7.4	Conclusion	82
8	Summary	83
	Bibliography	85
	Biography	101
	Acknowledgements	103

Chapter 1

Introduction

1.1 Preface

Magnetic thin films and multilayers have been intensively studied in various aspects for their importance in data storage and sensor applications as well as in fundamental physics. The most outstanding impact of magnetism occurs via spintronic devices, which consist of artificially structured magnetic materials. The fundamental magnetic properties of magnetic multilayers, e.g., magnetic anisotropy, giant magnetoresistance (GMR) and tunnel magnetoresistance (TMR) rely much on their interfacial conditions. Importance of the interface quality is especially highlighted for the multilayer system. Several multilayers composed of $3d$ metals are known to possess a characteristic property, which is expected to support a basic spintronic technology [1, 2, 3, 4]. For example, magnetic ordered alloys with a $L1_0$ -type crystal structure have been extensively studied as candidate new materials in many years, where the crystal structure contains an alternate arrangement of monoatomic layers of magnetic metals and noble metals with different magnetic properties [5, 6, 7, 8]. In a ferromagnetic (FM) multilayer system, through a non-magnetic spacer layer in between the two FM layers, the magnetically free FM layer interacts with the other FM layer whose magnetization is pinned by the exchange coupling with an antiferromagnetic (AFM) layer [9, 10]. The magnitude of the magnetic anisotropy energy, exchange bias or the spin-dependent transport properties could be significantly degraded by the local environment at interface such as atomic defects, roughness, intermixing, which could have drastic influence to overall properties [11, 12, 13].

1. INTRODUCTION

The size reduction enhances the importance of interfaces properties in regards to bulk ones.

One of the main goals of the research on such low-dimensional magnetism is to find correlations between the structure and the magnetic properties of ultrathin epitaxial films on the atomic scale. Detailed understanding of such a relationship is not only of basic interest but would allow us to tailor magnetic materials with desired properties. Up to now, several methods have been developed to investigate the local magnetic properties at interface of multilayer systems. The most advanced magnetic imaging techniques like magnetic force microscopy (MFM), scanning electron microscopy with polarization analysis (SEMPA) and photoemission electron microscope (PEEM) has been on the order of several nanometers (nm). However, these magnetic resolution are still far from the atomic scale. A transmission electron microscope (TEM) is also used to measure the local interfacial structure. However, the signal is an average over the film, which contribute leading to a cancellation of the signal in certain geometries. A perfect tool to study the interaction of the structural, electronic and magnetic properties of magnetic nanostructures is spin-polarized scanning tunneling microscopy/spectroscopy (SP-STM/STS). It combines the high lateral resolution of the STM/STS with spin sensitivity which allows not only the investigation of the very local environment but also the electronic origin which determines the magnetic properties in real space at the atomic level. Combining X-ray absorption spectroscopy/magnetic circular dichroism (XAS/XMCD) with SP-STM/STS, we address such local correlation of magnetic multilayer, even to buried layers at the interface.

As highly interesting model system to study the correlation of structural, electronic and magnetic properties in the vicinity of the AFM/FM interface, we adopted Mn/Fe thin film heterostructures as a probe multilayer. Fe is known to be the prototypical ferromagnet with body-centered-cubic (bcc) phase at room temperature, but between about 1185 K and 1667 K it is face-centered-cubic (fcc). However, due to a small lattice mismatch between fcc-Cu ($a_{\text{Cu}} = 3.61 \text{ \AA}$) and fcc-Fe ($a_{\text{fcc}}^{\text{Fe}} = 3.59 \text{ \AA}$), epitaxial growth of the Fe thin film grown on Cu(001) offers an unique opportunity to stabilize in a metastable structure. Since the magnetic phases of the Fe are energetically close, the Fe films are sensitive to the slight structural changes [14, 15, 16]. Therefore, Fe/Cu(001) has become an important prototype system for studying the

relation between structure and magnetism. And Mn film is grown on top of that as the AFM layer. Mn displays diverse phases on different crystalline lattices under different conditions. The stable bulk α -Mn shows a noncollinear antiferromagnetic structure [17]. Mn also accounts for the various magnetic properties in Mn-based alloys such as MnFe [11] and MnNi [18] which are widely used as pinning layers in spin valve devices. On the surface of low-dimensional Mn films, because of the broken inversion symmetry, unique magnetic spin structures might be found. Actually, Mn can be stabilized on bcc-Fe(001) whisker substrate in a body-centered tetragonal (bct) structure and shows an uncompensated collinear layerwise AFM structure revealed by SP-STM [19, 20, 21]. According to an *ab initio* study exhibits a tetragonal state of fcc-Mn has unique magnetic ground states, e.g. layered and in-plane antiferromagnetism [22]. Thus, in the Mn/Fe thin film heterostructures interfacial structure changes due to a formation of alloy can be expected and an epitaxy-stabilized metastable structure presents unique magnetic properties.

1.2 Purpose

In the vicinity of the interface, previous STM works have related the electronic and magnetic properties of single atom and molecule as a very well defined sample. On the other hand, the atomic scale investigation of the structural, electronic and magnetic properties of magnetic thin films on single crystal is more difficult due to the interfacial effects. While SP-STM studies on antiferromagnets have been carried out predominantly grown on single crystals, the studies of the AFM/FM multilayers which is more practical interest have rarely done so far.

In the present study, we combine SP-STM/STS and XAS/XMCD to reveal the roles of entangled interfacial factors and clarify the surface/interface magnetic structure of a FM film with an AFM overlayers on the atomic scale. As the FM layer, we chose fcc Fe thin films on Cu(001) due to their quite sensitive electronic and magnetic properties to structural changes on the surface. The Mn overlayers were chosen as the AFM layer with a thickness between 0.5 and 7 monolayer (ML). We carefully investigate the growth, intermixing, atomic structure and electronic structure of Mn thin films on fcc Fe thin films. Based on the observation, the roles of entangled interfacial factors characterizing electronic and magnetic properties of

1. INTRODUCTION

the entire system transition is clarified. Furthermore, the high lateral resolution with SP-STM could provide new insight into the details of the interfacial magnetic properties that is inaccessible in conventional interfacial magnetism studies.

1.3 Outline

The present work is organized as follows:

Chapter 2 introduces the the working principles of (SP-)STM/STS and XAS/XMCD. The experimental setup and sample preparation techniques are given in **Chap.3**. Experimental results on Mn/Fe thin film heterostructures on Cu(001) are presented in the chapters 4–7.

Chapter 4 is dedicated to the growth and magnetism of the Fe thin film on Cu(001). At first a review on previous results about Fe thin film grown Cu(001) surface is given. Then the results about thickness dependent STM and XAS/XMCD measurements are presented.

Chapter 5 focuses on the growth of the Mn thin film grown on fcc-Fe/Cu(001) surface studied by STM/STS. Thickness dependent STM/STS measurements reveal the changes of the structural and electronic properties due to the intermixing between Mn and Fe thin films at the interface.

Chapter 6 exhibits combining XAS and XMCD experiments with STM and STS measurements, leading to discussion on a dominant interfacial factor characterizing electronic and magnetic properties of the entire system dynamically changes with the thickness of the Mn overlayer.

Chapter 7 continues exploring the question raised in the previous chapter, regarding the magnetic properties of the Mn thin films. SP-STM/STS presents the atomic scale imaging reflecting spin structure and the spin-resolved electronic properties of the Mn surfaces.

Summary of the main experimental results obtained in the present work and conclusions of this thesis are presented at the end in **Chap. 8**.

Chapter 2

Experimental and theoretical background

2.1 Scanning tunneling microscopy and spectroscopy

Scanning tunneling microscopy (STM) is a powerful tool to study surfaces of conducting samples with an atomic resolution. The most obvious advantage of this technique is to obtain the correlations among of structural, electronic and magnetic properties with a high spatial and energy resolution. The STM consists of a metallic tip that is scanned closely above a sample surface. A voltage applied between tip and sample leads to tunneling current which is used to gather information about the surface. This section gives a short introduction to the basic principles of STM, scanning tunneling spectroscopy (STS) and also spin-polarized (SP-)STM.

2.1.1 History and concept

Since its invention by Gerd Binnig and Heinrich Rohrer [23, 24] at the laboratories of IBM in 1981 STM has developed into a powerful tool for surface characterization at an atomic scale. Thanks to its high spatial resolution STM opened a new field for investigating the physical properties of nanostructure/surfaces. Today, STM is widely used in surface science studies.

2. EXPERIMENTAL AND THEORETICAL BACKGROUND

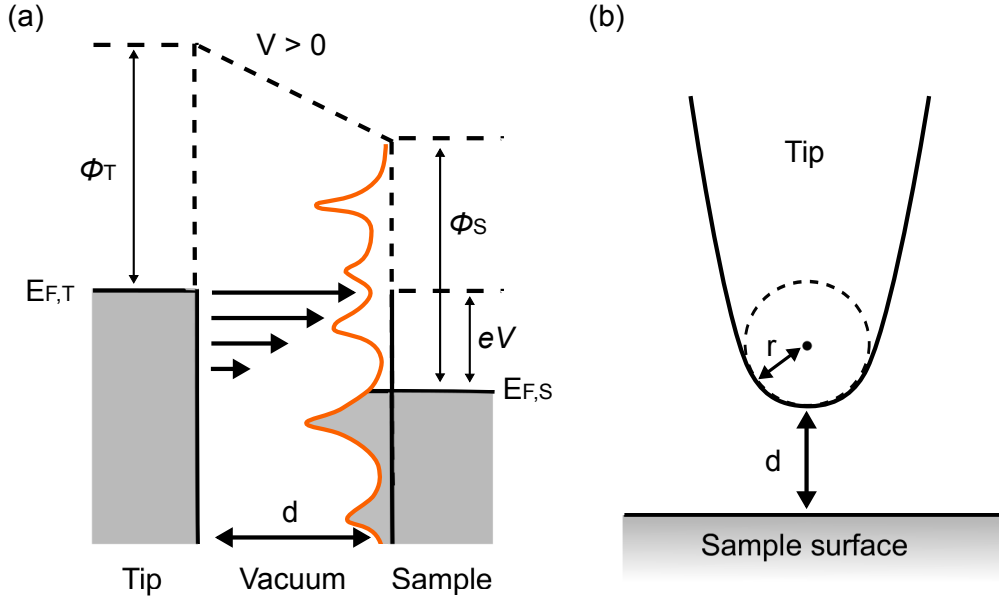


Figure 2.1: (a) Energy diagram for tunneling in STM. ϕ_T , ϕ_S are the work function and $E_{F,T}$, $E_{F,S}$ are the Fermi energies of tip and sample, respectively. At a positive bias as shown here the Fermi levels of the sample and tip are displaced by the bias applied and the electrons tunnel from the tip into the unoccupied states of the sample conduction band. (b) Tunneling geometry within the Tersoff-Hamann model. The tip is approximated by a s-like wave function at position r and the distance of nearest approach between tip sample surface is noted as d .

2.1.2 Topography

To introduce the STM working principle we consider an STM consisting of a sharp metallic tip and a sample surface. In a most simplistic model the tunnel process in an STM can be described in analogy to tunneling through a one-dimensional potential barrier. For a better understanding, Fig. 2.1 shows a system of the tip and surface in the STM geometry. The potential barrier in the STM geometry is the vacuum barrier between the tip and surface. When the tip is brought close enough to the surface, typically several angstrom (\AA), wave functions of the tip and sample overlap and a tunneling current, which depends exponentially on the width of the vacuum gap, flows between the tip and the sample. Applying a voltage (V) between tip and sample results in a tunneling current, which is described approximately by:

2.1 Scanning tunneling microscopy and spectroscopy

$$I_T \propto e^{-2kd} \quad (2.1)$$

where

$$k = \frac{\sqrt{2m(\phi - eV)}}{\hbar} \quad (2.2)$$

Here, d is the width of the vacuum gap and ϕ is the work function, with $V \ll \phi$. The voltage applied between the tip and sample is referred to as V . The work function of a metal surface is the minimum energy needed to remove an electron from the bulk into the vacuum outside the solid surface. For the sake of simplicity the work function is assumed to be the same for the tip and sample here. Figure 2.1(a) visualizes the content on the basis of one dimensional energy diagrams for tunneling in STM. Within this simple picture, the tunneling process is described as follow: When a positive voltage is applied to the sample, the Fermi energy of the sample shifts to a lower value with respect to the Fermi energy of the tip. Then only states that are located between the Fermi energy of the tip $E_{F,T}$ and $E_{F,T} - eV$ can contribute to the tunnel current. Occupied states of the tip which are close to the Fermi level $E_{F,T}$ contribute to I_T preferentially. The states away from the Fermi level contribute less to tunneling. The plotted arrows of different length represent the influence of the transmission coefficient arrows across the vacuum barrier as shown in Fig. 2.1(a). For a negative sample voltage the situation is reversed. In this case electrons tunnel from the occupied states of the sample into unoccupied states of the tip.

The analysis of the local tunneling current in STM measurements opened the possibility to image electronic structures on a surface at the atomic scale. The precise lateral and vertical movement of the tip during the scanning process in the STM measurements is controlled by piezoelectric actuators attached to the STM tip. These piezos change their length when a voltage is applied and the tip position can be precisely varied in the sub-angstrom scale. The most common mode for performing STM measurements is the constant current mode. In this case, the tip is stabilized at a fixed voltage applied between the tip and sample and a fixed tunneling current across the sample surface. Maintaining a constant tunneling current with a constant bias voltage the tip is scanned over the sample surface while the vertical position of the tip is adjusted by a feedback mechanism. By recording the changes

2. EXPERIMENTAL AND THEORETICAL BACKGROUND

of the vertical motion of the piezo required to maintain a constant current during the lateral motion, topographic STM image of the sample surface is obtained.

2.1.3 Spectroscopy

One of the most interesting aspects of the STM measurements is to obtain information about the electronic properties of the sample. For this purpose, the differential conductance dI/dV can be analyzed.

The model of Tersoff and Hamann assumes that the electronic structure of the tip is characterized by a metallic s -like orbital and that the applied voltages are much smaller than the work functions of tip and sample [25, 26]. With those assumptions and the geometry shown in Fig. 2.1(b) the tunneling current can be written as:

$$I_T \propto \int_0^{eV} \rho_S(E) \cdot \rho_T(E - eV) \cdot T(E, eV) dE \quad (2.3)$$

where ρ_S and ρ_T are the density of states (DOS) of the sample and tip, respectively. The coefficient $T(E, eV)$ is transmission probability between the sample and tip for the tunneling electrons. $T(E, eV)$ is given by

$$T(E, eV) = \exp \left[-d \cdot \sqrt{\frac{4m}{\hbar^2} (\phi_S + \phi_T + eV - 2E)} \right] \quad (2.4)$$

where ϕ_S and ϕ_T are the work function of sample and tip, respectively.

The local density of states (LDOS) of the sample can be retrieved from the voltage dependent derivative of the tunnel current $dI/dV(V)$ by differentiating Eq. 2.3 with the approximation that ϕ_T is constant results in

$$\frac{dI}{dV}(V) \propto \rho_S(eV) \cdot \rho_T(0) \cdot T(E, eV) + \int_0^{eV} \rho_S(E) \cdot \rho_T(E - eV) \cdot \frac{dT(E, eV)}{dV} dE \quad (2.5)$$

The second term can be often neglected and thus

$$\frac{dI}{dV}(V) \propto \rho_S(eV) \cdot \rho_T(0) \cdot T(E, eV) \quad (2.6)$$

2.1 Scanning tunneling microscopy and spectroscopy

In STS measurements, this is done by placing the tip over an interesting position with the stabilization parameters I_{Stab} and V_{Stab} . Then the feedback loop is switched off and the applied bias is ramped between an initial value and a final one. An open feedback loop leads to a fixed tip sample distance throughout the measurement. During the voltage ramp the tunnel current is recorded and an $I(V)$ spectrum is obtained at the fixed tip-sample distance.

In addition to $I(V)$, also the derivative dI/dV is measured simultaneously by a lock-in technique. The derivative dI/dV is within certain approximations proportional to the sample LDOS. It could be obtained by differentiating $I(V)$ curves numerically. However, this method is not preferable since it exhibits a smaller signal to noise ratio. The lock-in technique allows us to obtain the dI/dV signals with better signal to noise ratio. All dI/dV signals shown in this thesis were recorded using a lock-in technique with a modulation voltage of 20 mV and frequency of 733 Hz.

2.1.4 Spin polarized STM

Since the electron carries both charge and spin, STM-experiments allows to experimentally investigate not only the electronic but also the magnetic properties of nanostructures at surfaces at atomic-scale. To be sensitive to the spin dependent tunneling electrons of one electrode, the other electrode has to be spin-polarized as well. Slonczewski treated the problem of spin dependent tunneling between two spin-polarized electrodes theoretically [27]. Under the assumption of vanishing bias voltages and electrons behaving like free electrons within the conduction band, the spin-polarized tunnel current I_{SP} between two spin-polarized electrodes is given by

$$I_{\text{SP}}(V_0) = I_0(1 + P_{\text{S}} \cdot P_{\text{T}} \cdot \cos \theta) \quad (2.7)$$

where I_0 is the non-spin-polarized (spin-averaged) current. P_{S} (P_{T}) is the spin polarization of sample (tip). θ is the relative spin orientation of the magnetic moments of sample (\vec{m}_{S}) and tip (\vec{m}_{T}). Assuming a constant spin polarization of the tip (P_{T}), the tunnel current I_{SP} at a fixed position of the sample depends on the local spin polarization of the sample (P_{S}) and on variations of the angle (θ). The extreme

2. EXPERIMENTAL AND THEORETICAL BACKGROUND

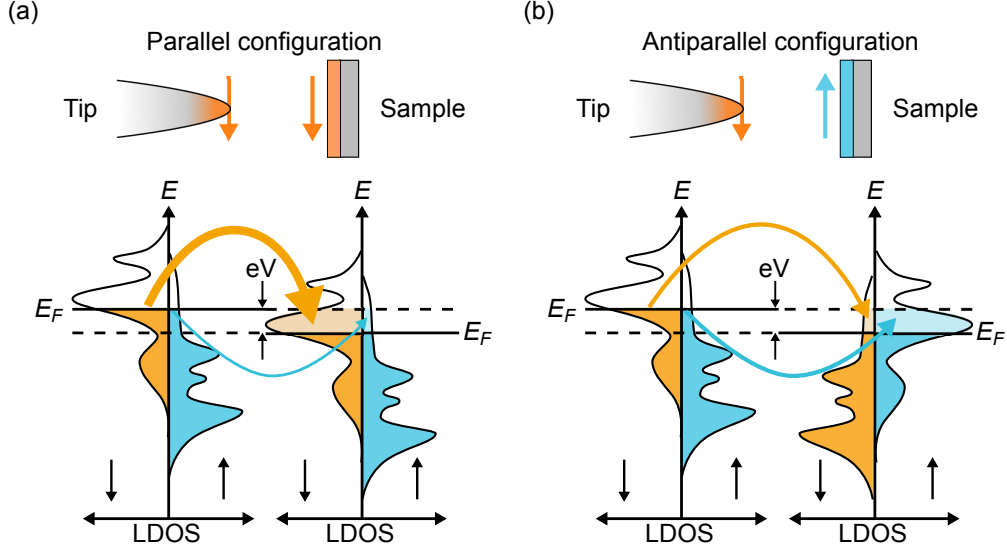


Figure 2.2: Spin-polarized tunneling between two ferromagnetic electrodes (tip and sample) for (a) parallel configuration of tip and sample magnetizations and (b) antiparallel configuration of their magnetization. The densities of states of the electrodes are split into up and down parts, respectively. The curved arrows indicate the tunneling current from left to right. The thickness of the arrows indicates tunneling probability.

cases of parallel ($\theta = 0^\circ$), vertical ($\theta = 90^\circ$) and antiparallel ($\theta = 180^\circ$) alignment of the magnetic moments of the tip and sample lead to the difference in the tunnel current:

$$I_{\text{SP}}(V_0) = I_0(1 + P_S \cdot P_T) \quad \text{for } \theta = 0^\circ \text{ (parallel)} \quad (2.8)$$

$$I_{\text{SP}}(V_0) = I_0 \quad \text{for } \theta = \pm 90^\circ \text{ (vertical)} \quad (2.9)$$

$$I_{\text{SP}}(V_0) = I_0(1 - P_S \cdot P_T) \quad \text{for } \theta = 180^\circ \text{ (antiparallel)} \quad (2.10)$$

Figure 2.2 presents a sketch of the spin polarized tunneling with spin split density of states. The spin orientation of the tunneling electrons is assumed to be conserved during tunneling, i.e. spin-up (spin-down) electrons always tunnel into spin-up (spin-down) states. The sketch in Fig. 2.2(a) shows the situation for a parallel configuration of the tip and sample magnetization. Considering an electron

2.1 Scanning tunneling microscopy and spectroscopy

with spin-up (spin-down) in an occupied tip state with a positive sample voltage V , electrons can tunnel into unoccupied spin-up (spin-down) states of the sample as indicated by the arrow. The high DOS of spin-down electrons at the Fermi energy of tip and sample leads to a high tunneling current. The contribution of spin-up electrons to the tunneling current is small, since fewer electrons and unoccupied sample states are available at the Fermi level. The sketch in 2.2(b) shows a reversed sample magnetization and spin polarization. In this configuration there are less unoccupied spin-down sample states available close to the Fermi energy, which leads to a low tunneling current of the spin-down electrons. For the spin-up electrons the situation remains unchanged. Since the tunneling probability depends on the number of electronic states available for the tunneling process the spin-polarized tunneling current will be larger for the parallel configuration of the magnetic electrodes than for the antiparallel one in the example of Fig 2.2(a) than in (b).

The spin dependence of the differential conductivity dI/dV can be explained by the same picture. Differentiation with respect to the bias voltage results in

$$\frac{dI}{dV}(V) \propto \frac{dI}{dV_{av}} (1 + P_S \cdot P_T \cdot \cos \theta) \quad (2.11)$$

where $\frac{dI}{dV_{av}}$ is the spin averaged dI/dV . The differential conductance (dI/dV) can be separated into a spin-averaged part and a spin-polarized part. In a similar way to the electronic dI/dV map, a magnetic dI/dV map of the sample can be acquired by choosing the appropriate bias voltage as contrast of the dI/dV signal on different magnetic domains.

Figure 2.3 shows how the local sample magnetization can be imaged by spin-polarized STS in the case of different tip magnetization. Figure 2.3(a) shows the angular dependence of the spin-polarized contribution to the dI/dV according to Eq. 2.11. Figure 2.3(b) and (c) show the measured differential conductance dI/dV above a sample with two in-plane magnetic domains and two out-of-plane magnetic domains using non-magnetic tip and magnetic tip, respectively. The measured dI/dV reflects the local configuration of the tip and sample magnetization. In Fig. 2.3(b) since the tip is non spin-polarized the dI/dV signals is constant on each domain. On the other hand, in Fig. 2.3(c) since the tip has a magnetization direction pointing in-plane three different level of dI/dV intensity can be observed.

2. EXPERIMENTAL AND THEORETICAL BACKGROUND

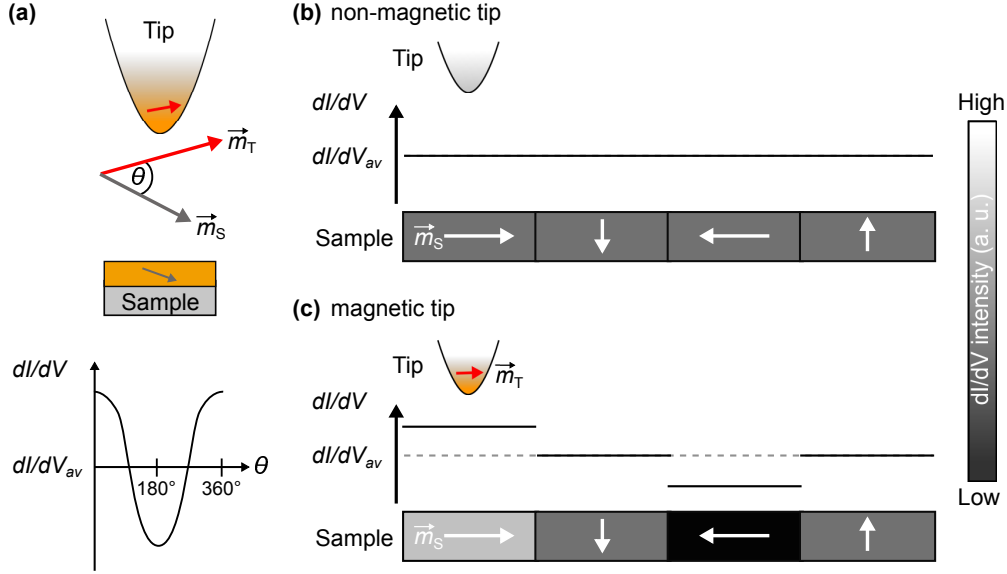


Figure 2.3: (a) Angular dependence of the spin-polarised dI/dV signal. \vec{m}_T and \vec{m}_S denote the spin orientation of the magnetic moments of tip and sample. (b) and (c) Response of the dI/dV to a sample with locally different magnetic orientation by assuming an electronically homogeneous surface with non-magnetic tip (b) and magnetic tip (c).

2.2 X-ray absorption spectroscopy

X-ray absorption spectroscopy (XAS) is a quantum mechanical process which involves the transition of core electrons to empty valence states. The transition probability per unit time from an initial state i to a final state f is given by Fermi's Golden rule. Hence, as the angular quantum number changes by ± 1 , the excitation of an electron from a p initial state only occurs into d and s orbitals. Considering the investigation of the $3d$ transition metals the absorption process involves excitations of photoelectrons from the $2p$ core levels to the unoccupied valence states. Moreover as the initial state is strongly localized to the core which has an atomic character, the XAS is an element specific method. In the present study, the XAS is carried out using total electron yield (TEY) detection. In the TEY mode all electrons emerging from the sample are detected, by measuring the current necessary to compensate for the lost charge by irradiation of the incident soft x-ray. TEY measurements are

limited to the near surface region, owing to the short electron escape depth, typically 5 nm. Therefore TEY measurements is surface sensitive.

2.3 X-ray magnetic circular dichroism

One of the most powerful techniques study localized magnetic moments in thin and multilayer films is x-ray magnetic circular dichroism (XMCD). This technique requires circular polarized x-rays and variation of photon energy range which are only fulfilled by synchrotron radiation facility. If the photoelectron is excited from a spin-orbit split core level, the $2p_{1/2}$ or the $2p_{3/2}$ level, the part of the photons angular momentum can be transferred to the spin of the electron via spin-orbit coupling. In ferromagnetic materials the majority spin band is more populated than the minority spin band, due to the exchange splitting as shown in Fig. 2.4(a). An imbalance of spin-up and spin-down populations in the $3d$ band leads to different absorption coefficients I^+ and I^- of right and left circularly polarized light at the $L_{2,3}$ edges. The information of the electronic and magnetic properties are thus contained in the XMCD, which is defined as the difference of the absorption coefficients $I^+ - I^-$. In Fig. 2.4(b), typical XAS and XMCD at the $L_{2,3}$ edges are illustrated. The clear advantage of XAS and XMCD in probing magnetism is the element specificity because the energy of absorption edges is characteristic for the different elements.

The XMCD sum rules can be used to separately determine the spin (m_{spin}) and orbital (m_{orb}) components of the magnetic moment [28, 29]. For the $2p \rightarrow 3d$ transitions of the $L_{2/3}$ edges the sum rules can be written as

$$m_{\text{orb}} = -\frac{2}{3} \frac{\int_{L_3+L_2} (I^+ - I^-) dE}{\int_{L_3+L_2} \left(\frac{I^+ + I^-}{2} - \mu^{BG}\right) dE} \frac{(10 - n_d)}{P_c} \quad (2.12)$$

$$m_{\text{spin}} + 7m_T = -\frac{6 \int_{L_3} (I^+ - I^-) dE - 4 \int_{L_3+L_2} (I^+ - I^-) dE}{\int_{L_3+L_2} \left(\frac{I^+ + I^-}{2} - I^{BG}\right) dE} \frac{(10 - n_d)}{P_c} \quad (2.13)$$

Both equations are given in units of μ_B/atom . I^{BG} is absorption background and n_d is the number of $3d$ electrons. The magnetic dipole moment m_T arises from a non-spherical spin distribution. From the experimental observation, the effective spin moment $m_{\text{spin}}^{\text{eff}}$ including m_T term as Eq. 2.13 can be obtained.

2. EXPERIMENTAL AND THEORETICAL BACKGROUND

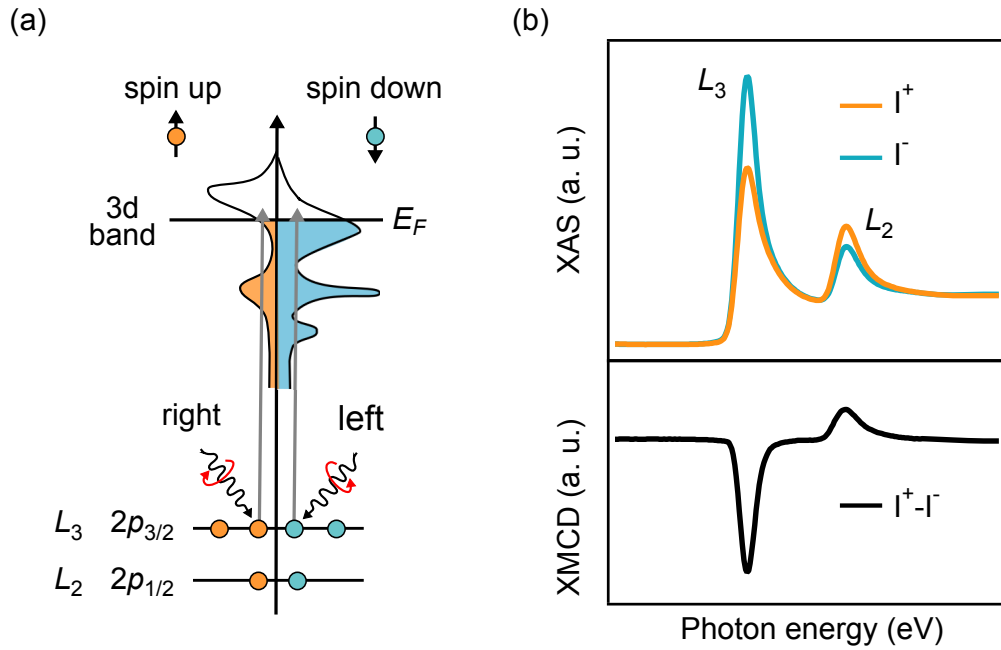


Figure 2.4: Illustration of an XMCD measurement, for L -edge absorption of a $3d$ magnetic metal. (a) Illustration of the the adsorption of circularly polarized photons in a $3d$ magnetic metal. (b) Experimental XAS at the L -edge obtained with right-circularly polarized x-rays for different orientations of the magnetization relative to the photon helicity.

Chapter 3

Instrumentation and Preparation

The aim of the present work is to study the clean and well-ordered magnetic films by means of STM/STS and XAS/XMCD. Therefore, the instrumental setup should ensure the cleanliness of the sample and repeatability of the experiments. For this reason the present studies have been performed in an ultra high vacuum (UHV) system, that is described in the present chapter. The specific characteristics of the UHV system, the STM and XAS/XMCD together with the sample preparation procedure are described in the following sections.

3.1 The ultra-high vacuum systems

The experiments were carried out in two independent UHV chambers for STM/STS and XAS/XMCD. Each system consists of three chambers separated by UHV valves: (i) a load-lock allowing tip and sample transfer into the system within several hours, (ii) a preparation chamber for tips and samples, and equipped with an Auger electron spectrometer (AES) and low energy electron diffraction (LEED), (iii) main chamber for STM/STS and XAS/XMCD measurements.

The samples can be easily and efficiently transferred and exchanged without breaking the vacuum. The pressure in the main chambers (less than 1×10^{-10} Torr) is achieved through a two-stage pumping system consisting of a turbo molecular pump and an ion sputter pump. Ti sublimation pump is also used to the inner part of the chamber walls, what helps to temporarily further decrease the pressure.

3. INSTRUMENTATION AND PREPARATION

3.1.1 Setup for scanning tunneling microscope

Figure 3.1 shows a photograph of the instrument including commercial an OMI-CRON low temperature (LT-) STM system. All the STM measurements described in this work were carried out with this STM situated inside the radiation shields connected to a liquid nitrogen (N_2) bath of the cryostat. The bath is surrounded by an additional nitrogen bath which increases the measurement time at 80 K to about 48 h. The tip is exchangeable in situ and mechanically clamped inside a piezo tube scanner using the coarse approach mechanism. The piezo tube can be moved by piezo motors in the x and y directions and moved in the z direction for the approach into the tunneling contact. A CCD camera helps to manually approach the tip to the sample before the automatic approach is used to get into tunneling contact. The STM chamber is connected to a fully equipped preparation chamber where we can clean the crystal surfaces and tip apexes, deposit metals on the surfaces, and perform the LEED measurements to characterize the surfaces. The topographic images are obtained using a constant tunneling current (I_T) mode at constant sample-bias voltages (V_S). The differential conductance of tunneling current, dI/dV , is recorded using a lock-in technique with a modulation voltage of 20 mV and frequency of 733 Hz.

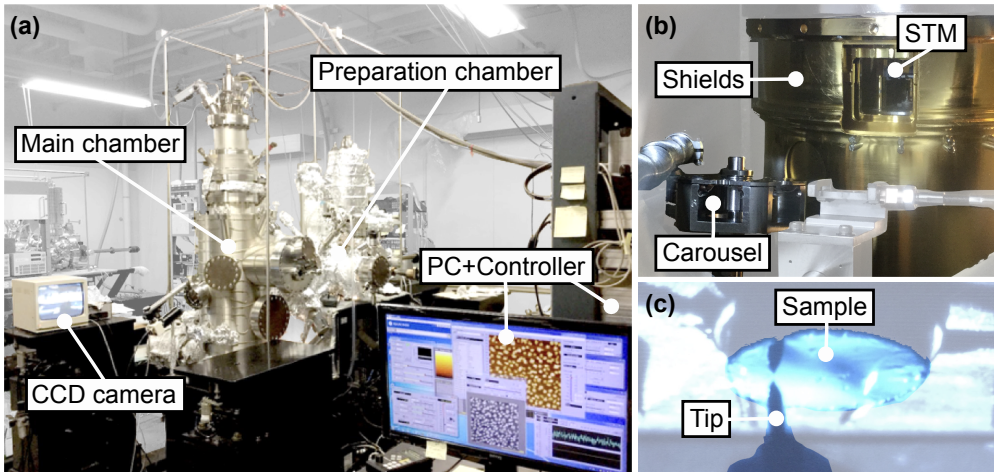


Figure 3.1: (a) Photograph of the UHV system. (b) View into the STM chamber. (c) View into the STM with CCD camera.

3.1.2 Setup for X-ray absorption spectroscopy

The XAS and XMCD measurements discussed in this thesis were performed at beamline (BL) 4B in Ultraviolet Synchrotron Orbital Radiation Facility (UVSOR)-III of Institute for Molecular Science (IMS). The beamline is a bending-magnet soft X-ray station equipped with a varied line spacing grating monochromator, which covers the photon energies of 25–1000 eV. The circular polarization of the incident X-ray is 65% and the X-ray propagation vector is set within the $(1\bar{1}0)$ plane of the Cu(001) substrate. The experimental setup, shown in Fig 3.2, consists in a series of connected UHV chambers. The main chamber for the measurements is equipped with a superconducting magnet with a coil made of a NbTi wire and magnetic field up to $B = \pm 5$ T can be achieved along the x-ray beam direction.

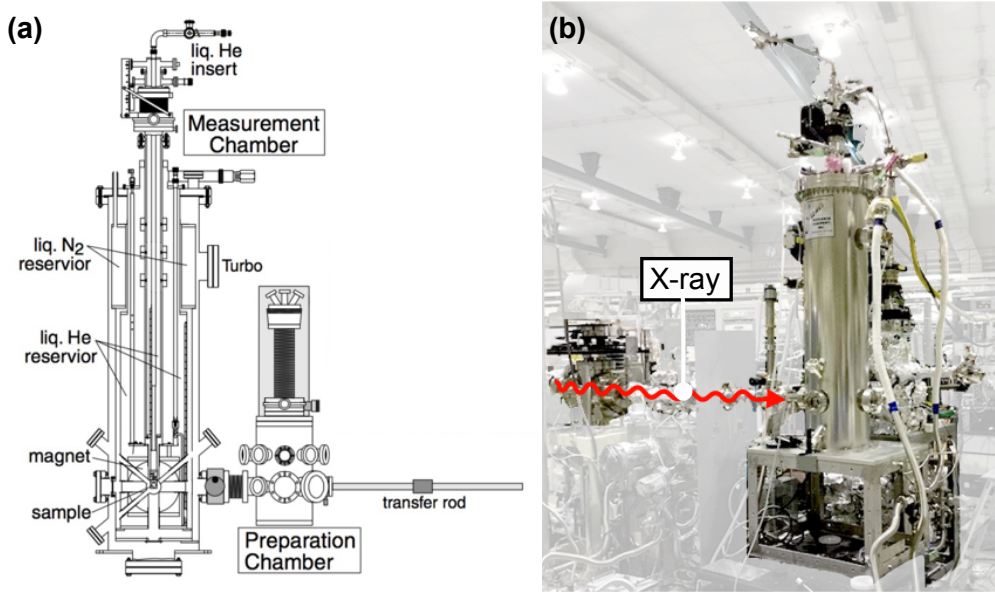


Figure 3.2: XAS/XMCD measurements setup in BL 4B at UVSOR (taken from Ref. [30]). (a) Schematic drawing of the measurements system. (b) Photograph of the UHV-system.

Absorption spectra were measured for parallel (I^+) and antiparallel (I^-) alignment of the photon helicity and the sample spin direction. Then, the XMCD spectrum was obtained by subtracting the former spectrum from the latter one. Mag-

3. INSTRUMENTATION AND PREPARATION

netic field B up to ± 5 T was applied parallel to the X-ray incidence direction at the angles $\theta = 0^\circ$ and 55° with respect to the surface normal. The spectra for normal ($\theta = 0^\circ$) and grazing ($\theta = 55^\circ$) incidence were sensitive to the out-of-plane and in-plane magnetizations of the samples, respectively. For the measurement of Fe magnetization curves, the value of the Fe L_3 and L_2 XAS peaks were recorded at 706 eV and 719 eV, respectively. The curve was obtained by taking the ratio of the two intensities as a function of magnetic field. The XAS and XMCD measurements were performed in an UHV ($< 8.0 \times 10^{-11}$ Torr) at 7 and 80 K. All the samples were prepared in an UHV chamber connected to measurement chamber via a gate valve.

3.2 Sample preparation

This section presents the experimental techniques to prepare sample surfaces studied and STM tips in this thesis. The first part of this section describes the preparation of the clean Cu(001) surface, and the deposition of Fe and Mn on Cu(001) surface using an electron-beam heating evaporator. The second part concentrates on the tip preparation via electrochemical etching and in-situ annealing, and describes the preparation of magnetic STM tips required for SP-STM measurements.

3.2.1 Substrate preparation

3.2.1.1 Cleaning the Cu(001) surface

A Cu(001) single crystal was used as the substrate in this study. Cu(001) is known to be one of the substrates suitable for epitaxy of magnetic metals. The crystal is mounted on a molybdenum sample holder [Fig. 3.3(a)]. After transferred onto a heating stage [Fig. 3.3(b)], the sample can be annealed by electron bombardment (EB) [Fig. 3.3(c)]. To achieve well-defined surfaces, the Cu(001) has been cleaned by several cycles of Ar^+ sputtering and subsequent annealing at 720 K. Cleanliness and orderliness of the surface lattice were evaluated by STM, AES and LEED. Figure 3.4(a) shows an STM image of a freshly prepared Cu(001) single crystal and a sharp (1×1) LEED pattern. The image reveals a surface divided into terraces by parallel steps. The STM image in Fig. 3.4(b) is taken on the surface of a terrace. The terrace is atomically flat, and several adsorbates can be observed. The inset shows a zoom

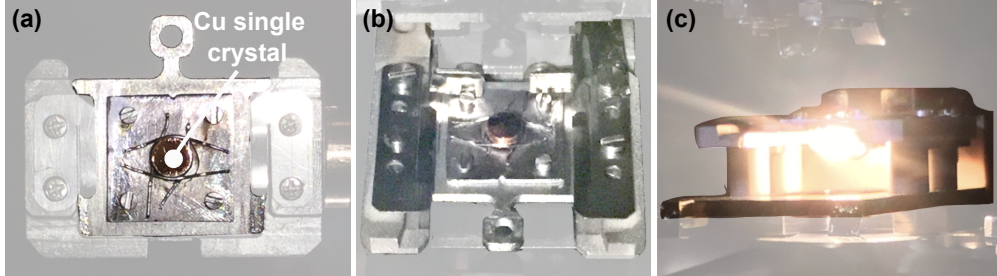


Figure 3.3: (a) Photograph of the Cu single crystal mounted on the sample holder. (b) Photograph of the sample on the heating stage. (c) Annealing the sample with electron bombardment from behind the sample.

in on one terrace with atomic resolution. The square lattice is clearly resolved. In AES spectra, only the characteristic peaks for Cu is seen [Fig. 3.4(c)]. The surface exhibits monoatomic steps with a step height of 180 pm as shown in Fig. 3.4(d). Figure 3.4(e) shows a dI/dV curve measured on bare Cu(001) surface. A peak is observed at -3.0 V, which is attributed to the onset of occupied Cu d-orbital states [31, 32, 33]. The peak at $+1.8$ V is either attributed to an unoccupied surface resonance or to the bulk band edge [32, 33, 34].

3.2.1.2 Deposition of the Fe and Mn

The Fe and Mn were deposited using electron-beam heating evaporators (Omicron EFM 3) [Fig. 3.5(a)] at a substrate temperature of 300 K. An Fe rod or Mn shots was heated by EB from a tungsten filament which has rather low work function facilitating the electron emission. A water-cooled copper shield avoids unwanted heating of the surrounding chamber wall that could cause impurities in the films. Mn (purity 99.99%) was evaporated from Mn shots surrounded by Ta wires, and Fe (purity 99.998%) was evaporated from a wire as shown in Fig. 3.5(b). To calibrate the evaporation rate, submonolayer amounts of the respective metals were deposited on a clean Cu(001) substrate at room temperature (RT), and the coverage was determined by STM as shown in Fig. 3.6. The growth rate of 0.8 monolayer (ML)/min was used during this work, respectively. We kept the vacuum below $< 3.0 \times 10^{-10}$ Torr during the deposition.

3. INSTRUMENTATION AND PREPARATION

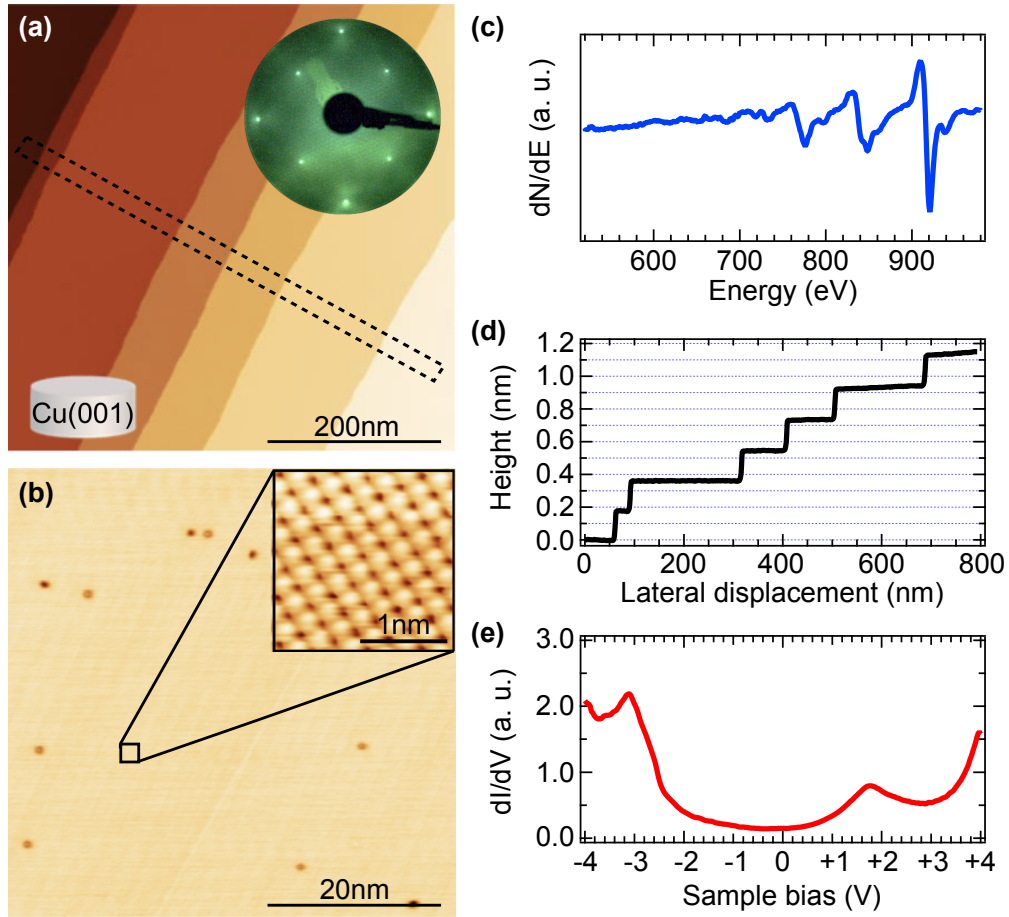


Figure 3.4: (a) Topographic image of a clean Cu(001) surface ($V_S = +1$ V, $I_T = 1$ nA). Inset in (a) is a LEED pattern of the Cu(001) substrate at the electron energy of 120 eV. (b) Magnified topographic image on the terrace ($V_S = +1$ V, $I_T = 1$ nA). Inset in (b) is an atomically resolved STM image of the square (1×1) lattice on a Cu(001) surface ($V_S = +30$ mV, $I_T = 10$ nA). (c) AES spectrum from the Cu(001) substrate. (d) Line-section taken along the box in (a). (e) dI/dV curve measured on the Cu(001) surface ($V_S = +4$ V, $I_T = 8$ nA).

3.2 Sample preparation

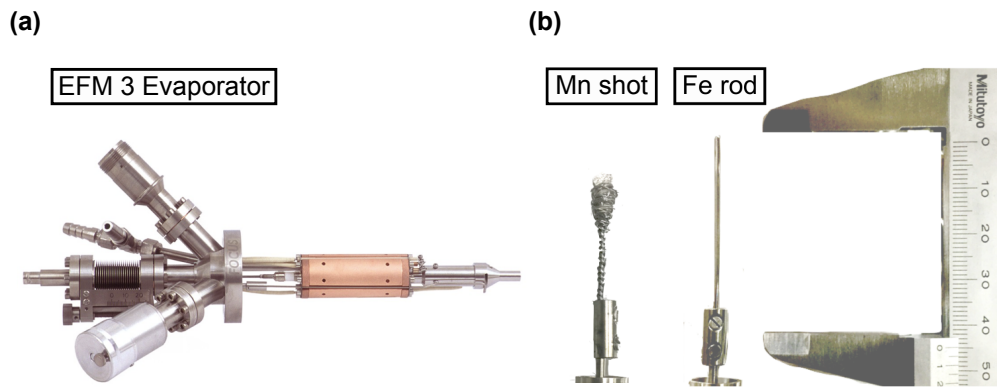


Figure 3.5: (a) Topographic image of a EFM 3 Evaporator. The figure is taken from Ref. [35]. (b) Mn and Fe sources in the evaporator.

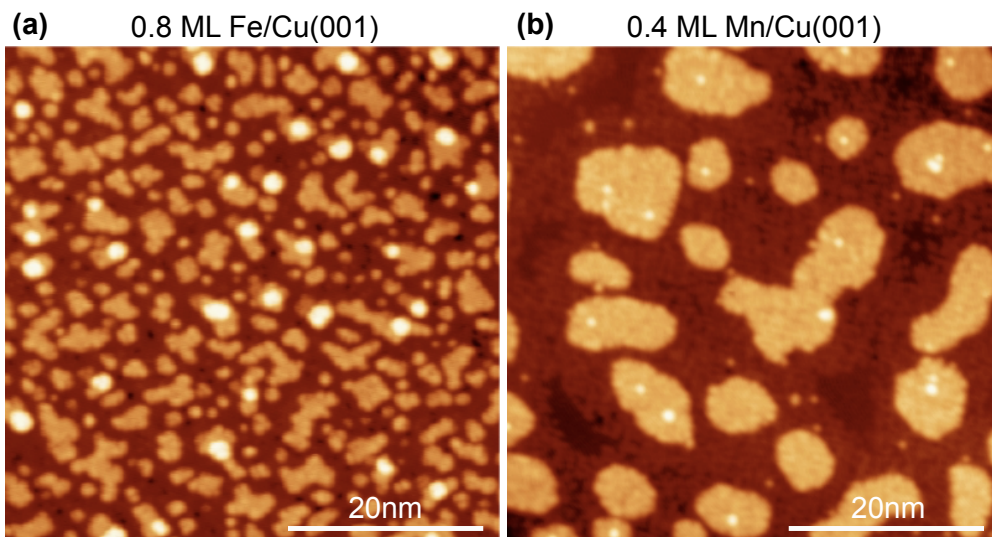


Figure 3.6: Determination of the Fe and Mn evaporation rate. Topographic image obtained after (a) Fe and (b) Mn evaporation onto the Cu(001) surface with evaporation times of 1 min and 30 sec, respectively.

3. INSTRUMENTATION AND PREPARATION

3.2.2 Tip preparation

For the spin-polarized STM observations, we prepared a Fe-covered W tip. We first electrochemically etched a polycrystalline W wire (0.3 mm) by using NaOH [Fig. 3.7(a), (b)]. The wire was positioned through a small flat ring where a drip of the solution was placed, forming a thin layer by surface tension. A potential difference was applied between the wire and the ring, which started the etching reaction. When the etching process finished, the bottom part of the wire dropped from the solution. With this method tip radii down to tens of nanometers (nm) have been achieved [36]. After the etching process, the tip was rinsed in a hot water and ethanol. Then, the tip was placed in the tip holder and fixed by pressing the tube [Fig. 3.7(c)]. Figure 3.7(d)-(f) show the W tips checked by Scanning Electron Microscope (SEM) immediately after the etching process.

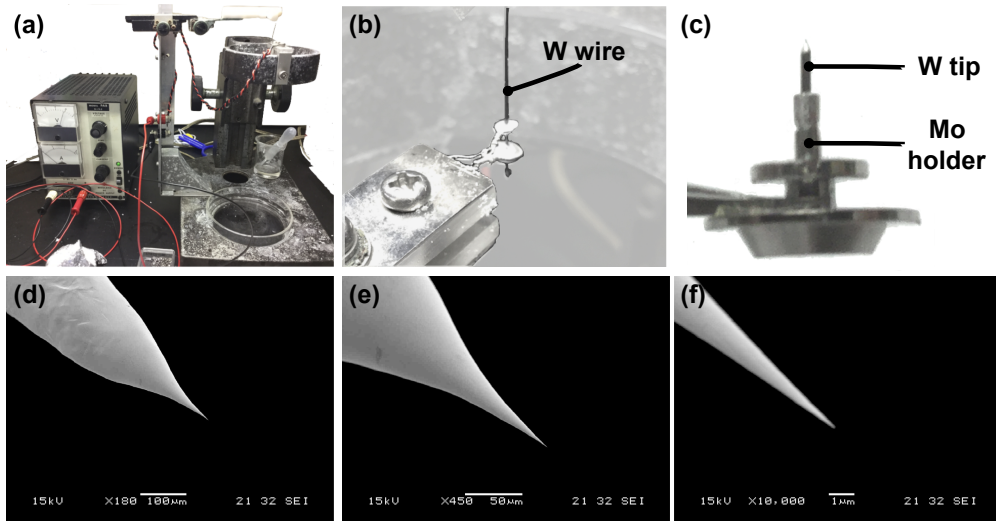


Figure 3.7: (a) Setup for electrochemical etching of STM tips. (b) Electrochemical etching of W-tip with NaOH. (c) A W-tip mounted to a Mo tube by pressing together the tube after inserting the tip. (d-f) SEM images of a sharp W-tip with different scale. Scale bars are (d) 100 μm , (e) 50 μm , (f) 1 μm .

After etching, the tip is mounted on a tip holder and is subsequently introduced into the UHV chamber via the load lock using a tip holder and a transfer holder as shown in Fig. 3.8(a) and (b). As the etching was performed in air, the tip surface

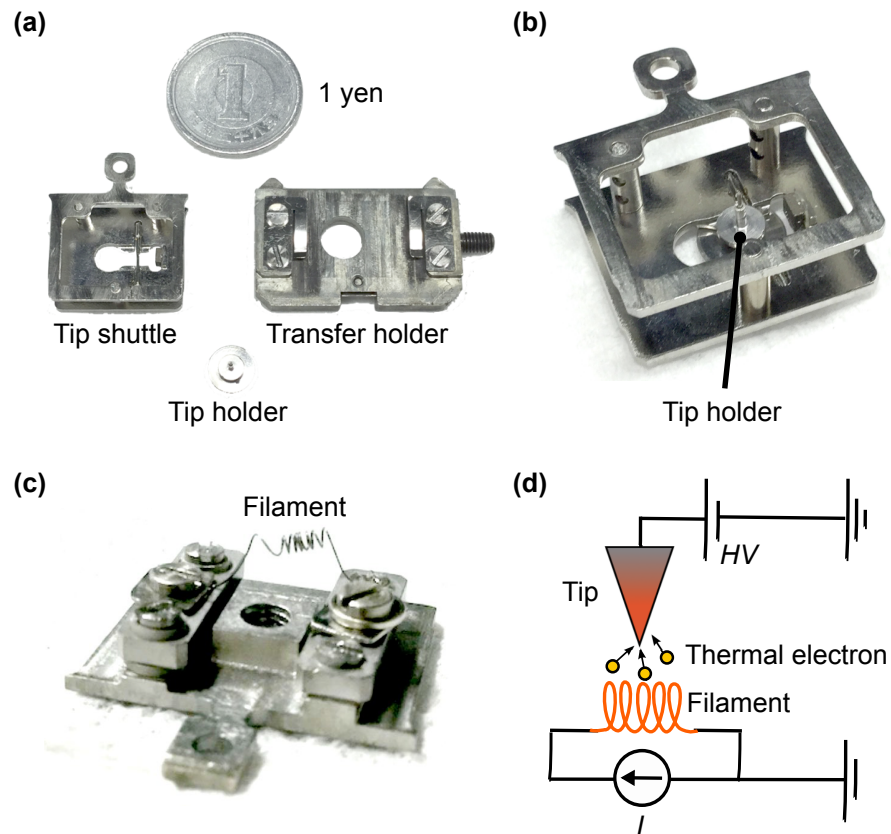


Figure 3.8: (a) Tip holder, tip shuttle and transfer holder for samples and tips. A one-yen coin indicates the size. (b) Tip shuttle mounting the tip holder fixed by permanent magnet. (c) W-filament for flushing the tips. (d) Circuit diagram for EB flushing.

was contaminated by oxides and/or other compounds. Such impurities would lead to unstable tunneling conditions in STM. To remove the oxide layer, it is cleaned by subsequent melting of the tip apex by EB, which also promotes a more stable configuration of the tip apex. Figure 3.8(c) shows the filament for EB heating. Figure 3.8(d) shows a simplified circuit diagram for EB heating. For flashing the tip, we applied high voltage potential to the tip, and electrons emitted by the filament were only accelerated to the tip. The photos shown in Fig. 3.9 were taken through viewport during EB heating.

3. INSTRUMENTATION AND PREPARATION

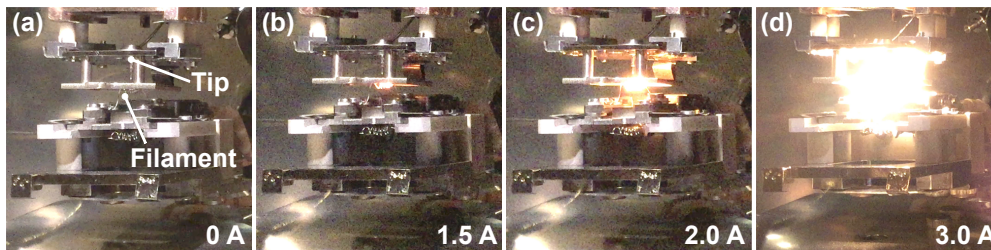


Figure 3.9: Flushing procedure for W tip with different current amps (a) 0 A. (b) 1.5 A. (c) 2.0 A. (d) 3.0 A.

3.2.2.1 Soft indentation (dipping of the tip)

In the beginning of each experiment, the tip was checked to make sure that it was free of multi tip features. For the spectroscopic measurements, a spectrum was taken on the clean sample surface to see if the surface state is imaged sharply and correctly. When the tip indicated multi features and the spectrum was featureless, the tip was dipped softly into the surface by 1 to 5 nm in the depth. Indenting the tip into the surface creates a hole in the surface as shown in Fig. 3.10.

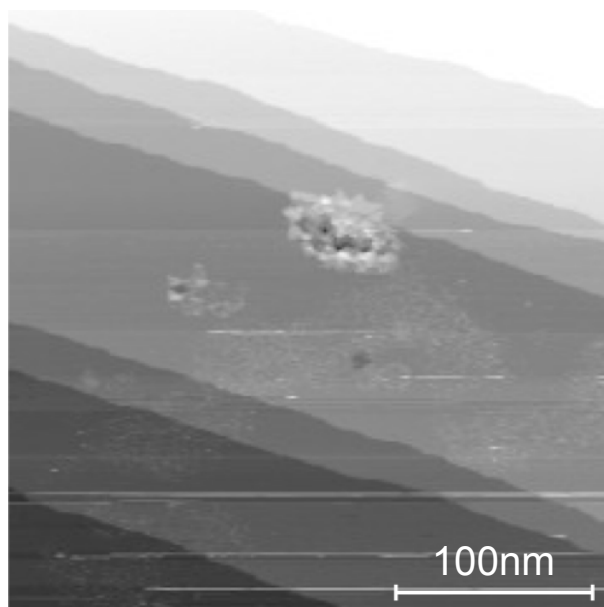


Figure 3.10: An STM image of the area around the center of a soft indentation.

3.2.2.2 Preparation of magnetic tips

In order to investigate magnetic properties of a surface with STM, a spin-polarised tip is required. For this purpose, the clean tungsten tips were coated with magnetic thin films and the choice of the materials determines the magnetic sensitivity of the tip. A thin Fe film covering the W tip is usually sensitive to the in-plane magnetization [19, 37, 38, 39, 40, 41, 42, 43, 44, 45]. Fabrication process of spin-polarized tip is shown in Fig. 3.11. A high-temperature flash up to 2200 K removes W oxides and other types of contaminations resulting from the electrochemical etching, and provides a clean metallic tip as described above. This is important for the subsequent thin-film deposition process because the evaporated magnetic layers adhere strongly to the tip only if the surface oxides have been removed completely. Otherwise, the magnetic layers are easily dropped off as the tip approaches the surface or during the scanning. As a result of the high temperature flash, the tip gets rather blunt. The influence of the heating can be imaged by the SEM before and after the treatment. Figure 3.12 shows the evolution of a W-tip in the process of several heating cycles. After preparing the clean W tips, a Fe thin film (20–40 ML) was deposited onto the tip apex at room temperature. Finally, the tip was mildly annealed to stabilize the Fe films on W tips.

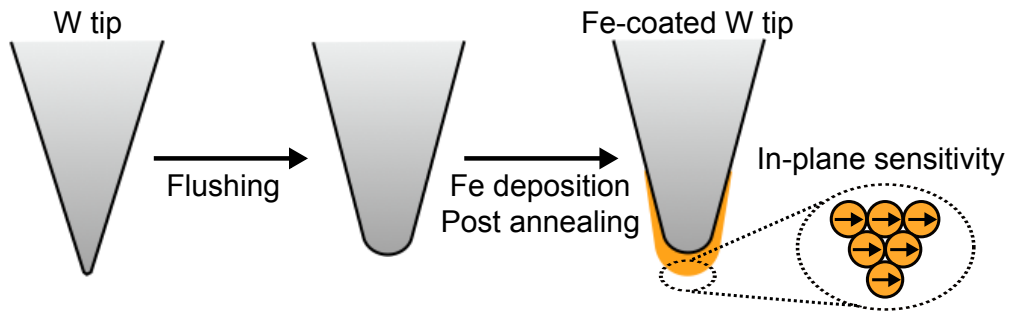


Figure 3.11: Fabrication process of spin-polarized tip. Schematic showing expected SP-STM tip configuration after Fe coverage.

3. INSTRUMENTATION AND PREPARATION

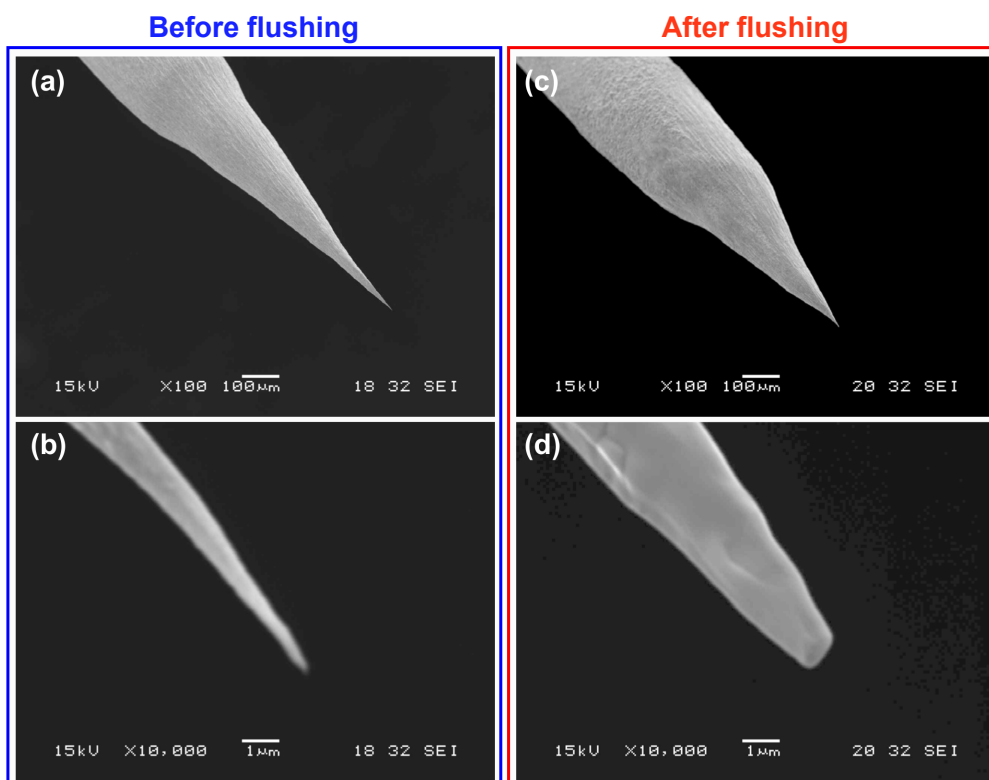


Figure 3.12: SEM images of the tips. (a) and (b) Before flushing, (c) and (d) after flushing.

Chapter 4

Growth and Magnetism of Fe/Cu(001)

Contents in this chapter will be published in five years and are not open to the publish now.

本章については、5年以内に雑誌等で刊行予定のため、現在は非公開。

Chapter 5

Growth of Mn/fcc-Fe(001)

Contents in this chapter will be published in five years and are not open to the public now.

本章については、5年以内に雑誌等で刊行予定のため、現在は非公開。

Chapter 6

Dynamic interface formation in magnetic thin film heterostructures

Contents in this chapter will be published in five years and are not open to the public now.

本章については、5年以内に雑誌等で刊行予定のため、現在は非公開。

Chapter 7

Observation of the surface and interface magnetism in Mn/Fe heterostructure

Contents in this chapter will be published in five years and are not open to the public now.

本章については、5年以内に雑誌等で刊行予定のため、現在は非公開。

Chapter 8

Summary

Contents in this chapter will be published in five years and are not open to the public now.

本章については、5年以内に雑誌等で刊行予定のため、現在は非公開。

Bibliography

- [1] T. Maruyama, Y. Shiota, T. Nozaki, K. Ohta, N. Toda, M. Mizuguchi, A. A. Tulapurkar, T. Shinjo, M. Shiraishi, S. Mizukami, Y. Ando and Y. Suzuki. Large voltage-induced magnetic anisotropy change in a few atomic layers of iron. *Nature Nanotechnology* **4**, 158 (2009).
- [2] B. G. Park, J. Wunderlich, X. Martí, V. Holý, Y. Kurosaki, M. Yamada, H. Yamamoto, A. Nishide, J. Hayakawa, H. Takahashi, A. B. Shick and T. Jungwirth. A spin-valve-like magnetoresistance of an antiferromagnet-based tunnel junction. *Nature Materials* **10**, 347 (2011).
- [3] W.-G. Wang, M. Li, S. Hageman and C. L. Chien. Electric-field-assisted switching in magnetic tunnel junctions. *Nature Materials* **11**, 64 (2012).
- [4] Y. Shiota, T. Nozaki, F. Bonell, S. Murakami, T. Shinjo and Y. Suzuki. Induction of coherent magnetization switching in a few atomic layers of FeCo using voltage pulses. *Nature Materials* **11**, 39 (2012).
- [5] M. Weisheit, S. Fähler, A. Marty, Y. Souche, C. Poinsignon and D. Givord. Electric Field Induced Modification of Magnetism in Thin-Film Ferromagnets. *Science* **315**, 349 (2007).
- [6] M. Ogiwara, S. Iihama, T. Seki, T. Kojima, S. Mizukami, M. Mizuguchi and K. Takanashi. Magnetization damping perpendicular of an $L1_0$ -FeNi thin film with peculiar magnetic anisotropy. *Applied Physics Letters* **103**, 242409 (2013).
- [7] N. Gaur, S. Kundu, S. N. Piramanayagam, S. L. Maurer, H. K. Tan, S. K. Wong, S. E. Steen, H. Yang and C. S. Bhatia. Lateral displacement induced

BIBLIOGRAPHY

- disorder in L1₀-FePt nanostructures by ion-implantation. *Scientific Reports* **3**, 1907 (2013).
- [8] A. Makino, P. Sharma, K. Sato, A. Takeuchi, Y. Zhang and K. Takenaka. Artificially produced rare-earth free cosmic magnet. *Scientific Reports* **5**, 16627 (2015).
- [9] A. E. Berkowitz and K. Takano. Exchange anisotropy — a review. *Journal of Magnetism and Magnetic Materials* **200**, 552 (1999).
- [10] J. Nogués and I. K. Schuller. Exchange bias. *Journal of Magnetism and Magnetic Materials* **192**, 203 (1999).
- [11] W. Kuch, L. I. Chelaru, F. Offi, J. Wang, M. Kotsugi and J. Kirschner. Tuning the magnetic coupling across ultrathin antiferromagnetic films by controlling atomic-scale roughness. *Nature Materials* **5**, 128 (2006).
- [12] E. Y. Tsymbal, O. N. Mryasov and P. R. LeClair. TOPICAL REVIEW: Spin-dependent tunnelling in magnetic tunnel junctions. *Journal of Physics Condensed Matter* **15**, R109 (2003).
- [13] C. Tiusan, J. Faure-Vincent, C. Bellouard, M. Hehn, E. Jouguelet and A. Schuhl. Interfacial Resonance State Probed by Spin-Polarized Tunneling in Epitaxial Fe/MgO/Fe Tunnel Junctions. *Physical Review Letters* **93**, 106602 (2004).
- [14] G. W. Fernando and B. R. Cooper. Theory of electronic structure and magnetic behavior of fcc iron grown on Cu(001). *Physical Review B* **38**, 3016 (1988).
- [15] D. Qian, X. F. Jin, J. Barthel, M. Klaua and J. Kirschner. Temperature-induced structure instability and magnetism of Fe/Cu(100). *Physical Review B* **66**, 172406 (2002).
- [16] T. Miyamachi, S. Nakashima, S. Kim, N. Kawamura, Y. Tatetsu, Y. Gohda, S. Tsuneyuki and F. Komori. Epitaxially stabilized iron thin films via effective strain relief from steps. *Physical Review B* **94**, 045439 (2016).

- [17] H. Yamagata and K. Asayama. NMR Study of Antiferromagnetic α -Mn Metal. *Journal of the Physical Society of Japan* **33**, 400 (1972).
- [18] M. F. Toney, M. G. Samant, T. Lin and D. Mauri. Thickness dependence of exchange bias and structure in MnPt and MnNi spin valves. *Applied Physics Letters* **81**, 4565 (2002).
- [19] T. K. Yamada, M. M. Bischoff, G. M. Heijnen, T. Mizoguchi and H. van Kempen. Observation of Spin-Polarized Surface States on Ultrathin bct Mn(001) Films by Spin-Polarized Scanning Tunneling Spectroscopy. *Physical Review Letters* **90**, 056803 (2003).
- [20] U. Schlickum, N. Janke-Gilman, W. Wulfhekel and J. Kirschner. Step-Induced Frustration of Antiferromagnetic Order in Mn on Fe(001). *Physical Review Letters* **92**, 107203 (2004).
- [21] U. Schlickum, C. L. Gao, W. Wulfhekel, J. Henk, P. Bruno and J. Kirschner. Effect of antiferromagnetic layers on the spin-dependent transport in magnetic tunnel junctions. *Physical Review B* **74**, 054409 (2006).
- [22] J. Hafner and D. Spišák. Ab initio investigation of the magnetism of tetragonal Mn: Bulk, surface, ultrathin films, and multilayers. *Physical Review B* **72**, 144420 (2005).
- [23] G. Binnig, H. Rohrer, C. Gerber and E. Weibel. Surface Studies by Scanning Tunneling Microscopy. *Physical Review Letters* **49**, 57 (1982).
- [24] G. Binnig, H. Rohrer, C. Gerber and E. Weibel. Tunneling through a controllable vacuum gap. *Applied Physics Letters* **40**, 178 (1982).
- [25] J. Tersoff and D. R. Hamann. Theory and Application for the Scanning Tunneling Microscope. *Physical Review Letters* **50**, 1998 (1983).
- [26] J. Tersoff and D. R. Hamann. Theory of the scanning tunneling microscope. *Physical Review B* **31**, 805 (1985).
- [27] J. C. Slonczewski. Conductance and exchange coupling of two ferromagnets separated by a tunneling barrier. *Physical Review B* **39**, 6995 (1989).

BIBLIOGRAPHY

- [28] B. T. Thole, P. Carra, F. Sette and G. van der Laan. X-ray circular dichroism as a probe of orbital magnetization. *Physical Review Letters* **68**, 1943 (1992).
- [29] C. T. Chen, Y. U. Idzerda, H.-J. Lin, N. V. Smith, G. Meigs, E. Chaban, G. H. Ho, E. Pellegrin and F. Sette. Experimental Confirmation of the X-Ray Magnetic Circular Dichroism Sum Rules for Iron and Cobalt. *Physical Review Letters* **75**, 152 (1995).
- [30] T. Nakagawa, Y. Takagi, Y. Matsumoto and T. Yokoyama. Enhancements of Spin and Orbital Magnetic Moments of Submonolayer Co on Cu(001) Studied by X-ray Magnetic Circular Dichroism Using Superconducting Magnet and Liquid He Cryostat. *Japanese Journal of Applied Physics* **47**, 2132 (2008).
- [31] C. Baldacchini, L. Chiodo, F. Allegretti, C. Mariani, M. G. Betti, P. Monachesi and R. del Sole. Cu(100) surface:High-resolution experimental and theoretical band mapping. *Physical Review B* **68**, 195109 (2003).
- [32] C. D. Ruggiero, T. Choi and J. A. Gupta. Tunneling spectroscopy of ultrathin insulating films: CuN on Cu(100). *Applied Physics Letters* **91**, 253106 (2007).
- [33] T. Choi, C. D. Ruggiero and J. A. Gupta. Tunneling spectroscopy of ultrathin insulating Cu₂N films, and single Co adatoms. *Journal of Vacuum Science & Technology B* **27**, 887 (2009).
- [34] D. P. Woodruff, S. L. Hulbert, P. D. Johnson and N. V. Smith. Unoccupied surface resonance on Cu(100) and the effect of vacuum-level pinning. *Physical Review B* **31**, 4046 (1985).
- [35] UHV-Evaporator : EFM 3, FOCUS GmbH, <http://www.focus-gmbh.com> .
- [36] J. P. Ibe, P. P. Bey, Jr., S. L. Brandow, R. A. Brizzolara, N. A. Burnham, D. P. Dilella, K. P. Lee, C. R. K. Marrian and R. J. Colton. On the electrochemical etching of tips for scanning tunneling microscopy. *Journal of Vacuum Science & Technology A* **8**, 3570 (1990).
- [37] H. J. Elmers, T. Furubayashi, M. Albrecht and U. Gradmann. Analysis of magnetic anisotropies in ultrathin films by magnetometry in situ in UHV. *Journal of Applied Physics* **70**, 5764 (1991).

-
- [38] M. Bode, R. Pascal and R. Wiesendanger. Scanning tunneling spectroscopy of Fe/W(110) using iron covered probe tips. *Journal of Vacuum Science & Technology A* **15**, 1285 (1997).
- [39] S. Heinze, M. Bode, A. Kubetzka, O. Pietzsch, X. Nie, S. Blügel and R. Wiesendanger. Real-Space Imaging of Two-Dimensional Antiferromagnetism on the Atomic Scale. *Science* **288**, 1805 (2000).
- [40] M. Bode. Spin-polarized scanning tunnelling microscopy. *Reports on Progress in Physics* **66**, 523 (2003).
- [41] K. von Bergmann, M. Bode and R. Wiesendanger. Magnetism of iron on tungsten (001) studied by spin-resolved scanning tunneling microscopy and spectroscopy. *Physical Review B* **70**, 174455 (2004).
- [42] T. Irisawa, T. K. Yamada and T. Mizoguchi. Spin polarization vectors of field emitted electrons from Fe/W tips. *New Journal of Physics* **11**, 113031 (2009).
- [43] R. Wiesendanger. Spin mapping at the nanoscale and atomic scale. *Reviews of Modern Physics* **81**, 1495 (2009).
- [44] S. Nagai, K. Hata, H. Oka, D. Sander and J. Kirschner. Atomic structure and spin polarization at the apex of tips used in spin-polarized scanning tunneling microscopy. *Applied Physics Express* **7**, 025204 (2014).
- [45] M. Haze, Y. Yoshida and Y. Hasegawa. Role of the substrate in the formation of chiral magnetic structures driven by the interfacial Dzyaloshinskii-Moriya interaction. *Physical Review B* **95**, 060415(R) (2017).
- [46] V. L. Moruzzi, P. M. Marcus, K. Schwarz and P. Mohn. Ferromagnetic phases of bcc and fcc Fe, Co, and Ni. *Physical Review B* **34**, 1784 (1986).
- [47] V. L. Moruzzi, P. M. Marcus and J. Kübler. Magnetovolume instabilities and ferromagnetism versus antiferromagnetism in bulk fcc iron and manganese. *Physical Review B* **39**, 6957 (1989).
- [48] J. Thomassen, F. May, B. Feldmann, M. Wuttig and H. Ibach. Magnetic live surface layers in Fe/Cu(100). *Physical Review Letters* **69**, 3831 (1992).

BIBLIOGRAPHY

- [49] S. Müller, P. Bayer, C. Reischl, K. Heinz, B. Feldmann, H. Zillgen and M. Wuttig. Structural Instability of Ferromagnetic fcc Fe Films on Cu(100). *Physical Review Letters* **74**, 765 (1995).
- [50] P. Xhonneux and E. Courtens. Direct correlation between the structure and magnetism of thin epitaxial Fe on Cu(100). *Physical Review B* **46**, 556(R) (1992).
- [51] M. Wuttig, B. Feldmann, J. Thomassen, F. May, H. Zillgen, A. Brodde, H. Hannemann and H. Neddermeyer. Structural transformations of fcc iron films on Cu(100). *Surface Science* **291**, 14 (1993).
- [52] P. Schmailzl, K. Schmidt, P. Bayer, R. Döll and K. Heinz. The structure of thin epitaxial Fe films on Cu(100) in the transition range fcc to bcc. *Surface Science* **312**, 73 (1994).
- [53] S. Müller, P. Bayer, A. Kinne, P. Schmailzl and K. Heinz. High precision LEED structure analysis of ultra-thin epitaxial fcc Fe films on Cu(100). *Surface Science* **322**, 21 (1995).
- [54] S. Müller, P. Bayer, A. Kinne, C. Reischl, R. Metzler and K. Heinz. Structure and stability of fcc Fe films on Cu(100) for coverages below five monolayers. *Surface Science* **331**, 723 (1995).
- [55] K. Heinz, S. Müller and P. Bayer. Iron multilayers on Cu(100) - a case of complex reconstruction investigated by quantitative LEED. *Surface Science* **352**, 942 (1996).
- [56] T. Bernhard, M. Baron, M. Gruyters and H. Winter. Surface Structure of Ultrathin Fe Films on Cu(001) Revisited. *Physical Review Letters* **95**, 087601 (2005).
- [57] A. Brodde and H. Neddermeyer. Scanning tunneling microscopy on the growth of Fe films on Cu(100). *Surface Science* **287**, 988 (1993).
- [58] J. Giergiel, J. Kirschner, J. Landgraf, J. Shen and J. Woltersdorf. Stages of structural transformation in iron thin film growth on copper (100). *Surface Science* **310**, 1 (1994).

- [59] A. Biedermann, M. Schmid and P. Varga. Nucleation of bcc Iron in Ultrathin fcc Films. *Physical Review Letters* **86**, 464 (2001).
- [60] A. Biedermann, R. Tscheliessnig, M. Schmid and P. Varga. Crystallographic Structure of Ultrathin Fe Films on Cu(100). *Physical Review Letters* **87**, 086103 (2001).
- [61] D. Qian, X. F. Jin, J. Barthel, M. Klaua and J. Kirschner. Spin-Density Wave in Ultrathin Fe Films on Cu(100). *Physical Review Letters* **87**, 227204 (2001).
- [62] X. F. Jin. Morphology and magnetic structure of Fe/Cu(100). *Journal of Physics D Applied Physics* **35**, 2332 (2002).
- [63] A. Biedermann, R. Tscheliessnig, M. Schmid and P. Varga. Local atomic structure of ultra-thin Fe films grown on Cu(100). *Applied Physics A: Materials Science & Processing* **78**, 807 (2004).
- [64] D. Li, M. Freitag, J. Pearson, Z. Q. Qiu and S. D. Bader. Magnetic phases of ultrathin Fe grown on Cu(100) as epitaxial wedges. *Physical Review Letters* **72**, 3112 (1994).
- [65] A. Berger, B. Feldmann, H. Zillgen and M. Wuttig. Correlation between the microscopic and macroscopic magnetic properties in ultrathin Fe/Cu(100)-films. *Journal of Magnetism and Magnetic Materials* **183**, 35–41 (1998).
- [66] J. H. Dunn, D. Arvanitis and N. Mårtensson. Magnetism of thin Fe films on Cu(100). *Physical Review B* **54**, R11157 (1996).
- [67] K. Yaji, M. Sawada, H. Namatame, T. Moko, M. Nagira, T. Ueno, A. Kimura and M. Taniguchi. Modification of structural and magnetic properties for Fe/Cu(001) by Cr adsorbates. *Physical Review B* **76**, 214403 (2007).
- [68] H. Abe, K. Amemiya, D. Matsumura, J. Miyawaki, E. O. Sako, T. Ohtsuki, E. Sakai and T. Ohta. Anomalous magnetic phases in Fe/Cu(001) ultrathin films induced by CO adsorption. *Physical Review B* **77**, 054409 (2008).

BIBLIOGRAPHY

- [69] M. Sawada, T. Ueno, T. Tagashira, H. Namatame and M. Taniguchi. XMCD experimental station optimized for ultrathin magnetic films at HiSOR-BL14. In R. Garrett, I. Gentle, K. Nugent and S. Wilkins (eds.) *American Institute of Physics Conference Series*, vol. 1234, 939 (2010).
- [70] D. A. Steigerwald, I. Jacob and W. F. Egelhoff. Structural study of the epitaxial growth of fcc-Fe films, sandwiches, and superlattices on Cu(100). *Surface Science* **202**, 472 (1988).
- [71] T. Detzel, N. Memmel and T. Fauster. Growth of ultrathin iron films on Cu(001): an ion-scattering spectroscopy study. *Surface Science* **293**, 227 (1993).
- [72] P. Bayer, S. Müller, P. Schmailzl and K. Heinz. Nonpseudomorphic and surface-reconstructed ultrathin epitaxial fcc Fe films on Cu(100). *Physical Review B* **48**, 17611 (1993).
- [73] T. Asada and S. Blügel. Total Energy Spectra of Complete Sets of Magnetic States for fcc-Fe Films on Cu(100). *Physical Review Letters* **79**, 507 (1997).
- [74] L. M. Sandratskii. Stable and variable features of the magnetic structure of fcc Fe/Cu(001) films. *Physical Review B* **81**, 064417 (2010).
- [75] J. Thomassen, B. Feldmann and M. Wuttig. Growth, structure and morphology of ultrathin iron films on Cu(100). *Surface Science* **264**, 406 (1992).
- [76] K. Yaji, M. Sawada, T. Moko, M. Nagira, T. Ueno, A. Kimura, H. Namatame and M. Taniguchi. Cr adsorption effect of magnetic property of Fe/Cu(001). *e-Journal of Surface Science and Nanotechnology* **4**, 345 (2006).
- [77] H. L. Meyerheim, J.-M. Tonnerre, L. Sandratskii, H. C. N. Tolentino, M. Przybylski, Y. Gabi, F. Yildiz, X. L. Fu, E. Bontempi, S. Grenier and J. Kirschner. New Model for Magnetism in Ultrathin fcc Fe on Cu(001). *Physical Review Letters* **103**, 267202 (2009).
- [78] J. Miyawaki, A. Chainani, Y. Takata, M. Mulazzi, M. Oura, Y. Senba, H. Ohashi and S. Shin. Out-of-Plane Nesting Driven Spin Spiral in Ultrathin Fe/Cu(001) Films. *Physical Review Letters* **104**, 066407 (2010).

-
- [79] M. N. Baibich, J. M. Broto, A. Fert, F. Nguyen van Dau, F. Petroff, P. Etienne, G. Creuzet, A. Friederich and J. Chazelas. Giant magnetoresistance of (001)Fe/(001)Cr magnetic superlattices. *Physical Review Letters* **61**, 2472 (1988).
- [80] S. A. Wolf, D. D. Awschalom, R. A. Buhrman, J. M. Daughton, S. von Molnár, M. L. Roukes, A. Y. Chtchelkanova and D. M. Treger. Spintronics: A Spin-Based Electronics Vision for the Future. *Science* **294**, 1488 (2001).
- [81] H. Zabel. Progress in spintronics. *Superlattices and Microstructures* **46**, 541 (2009).
- [82] B. Dieny. Giant magnetoresistance in spin-valve multilayers. *Journal of Magnetism and Magnetic Materials* **136**, 335 (1994).
- [83] J. Nogués, J. Sort, V. Langlais, V. Skumryev, S. Suriñach, J. S. Muñoz and M. D. Baró. Exchange bias in nanostructures. *Physics Reports* **422**, 65 (2005).
- [84] A. Davies, J. A. Stroscio, D. T. Pierce and R. J. Celotta. Atomic-Scale Observations of Alloying at the Cr-Fe(001) Interface. *Physical Review Letters* **76**, 4175 (1996).
- [85] A. Davies, J. A. Stroscio, D. T. Pierce, J. Unguris and R. J. Celotta. Observations of alloying in the growth of Cr on Fe(001). *Journal of Magnetism and Magnetic Materials* **165**, 82 (1997).
- [86] M. M. J. Bischoff, T. Yamada, A. J. Quinn and H. van Kempen. Scanning tunneling microscopy and spectroscopy study on the submonolayer growth of Mn on Fe(001). *Surface Science* **501**, 155 (2002).
- [87] T. K. Yamada, M. M. J. Bischoff, T. Mizoguchi and H. van Kempen. STM and STS study of ultrathin Mn layers on Fe(001). *Surface Science* **516**, 179 (2002).
- [88] C. E. ViolBarbosa, H. L. Meyerheim, E. Jal, J.-M. Tonnerre, M. Przybylski, L. M. Sandratskii, F. Yildiz, U. Staub and J. Kirschner. Inhomogeneous temperature dependence of the magnetization in fcc-Fe on Cu(001). *Physical Review B* **85**, 184414 (2012).

BIBLIOGRAPHY

- [89] T. Flores, M. Hansen and M. Wuttig. Structure and growth of Mn on Cu(100). *Surface Science* **279**, 251 (1992).
- [90] J. Song, C.-B. Wu, B. Zhang, J. Xu and W. Kuch. Layer-dependent properties and noncollinear spin structure of epitaxial antiferromagnetic Mn films on Co/Cu (001). *Physical Review B* **91**, 214406 (2015).
- [91] M. Bode, S. Heinze, A. Kubetzka, O. Pietzsch, M. Hennefarth, M. Getzlaff, R. Wiesendanger, X. Nie, G. Bihlmayer and S. Blügel. Structural, electronic, and magnetic properties of a Mn monolayer on W(110). *Physical Review B* **66**, 014425 (2002).
- [92] J. T. Kohlhepp, H. Wieldraaijer and W. J. M. de Jonge. Exchange anisotropy as a probe of antiferromagnetism in expanded face-centered-tetragonal Mn(001) layers. *Applied Physics Letters* **89**, 032507 (2006).
- [93] B.-Y. Wang, J.-Y. Hong, N.-Y. Jih, K.-H. Ou Yang, L.-R. Chen, H.-J. Lin, Y.-L. Chan, D.-H. Wei and M.-T. Lin. Probing magnetoelastic effects of ultrathin antiferromagnets via magnetic domain imaging in ferromagnetic-antiferromagnetic bilayers. *Physical Review B* **90**, 224424 (2014).
- [94] W. Weber, C. H. Back, U. Ramsperger, A. Vaterlaus and R. Allenspach. Submonolayers of adsorbates on stepped Co/Cu(100): Switching of the easy axis. *Physical Review B* **52**, 14400(R) (1995).
- [95] S. Hope, E. Gu, B. Choi and J. A. C. Bland. Spin Engineering in Ultrathin Cu/Co/Cu(110). *Physical Review Letters* **80**, 1750 (1998).
- [96] B.-C. Choi, P. J. Bode and J. A. C. Bland. Magnetic anisotropy strength and surface alloy formation in Mn/Co/Cu(001) overlayers. *Physical Review B* **59**, 7029 (1999).
- [97] M. A. Torija, J. P. Pierce and J. Shen. Magnetic capping layer induced spin reorientation: Co on Fe/Cu(100). *Physical Review B* **63**, 092404 (2001).

- [98] D. Matsumura, T. Yokoyama, K. Amemiya, S. Kitagawa and T. Ohta. X-ray magnetic circular dichroism study of spin reorientation transitions of magnetic thin films induced by surface chemisorption. *Physical Review B* **66**, 024402 (2002).
- [99] D. Sander, W. Pan, S. Ouazi, J. Kirschner, W. Meyer, M. Krause, S. Müller, L. Hammer and K. Heinz. Reversible H-Induced Switching of the Magnetic Easy Axis in Ni/Cu(001) Thin Films. *Physical Review Letters* **93**, 247203 (2004).
- [100] I. Yamamoto, T. Nakagawa, Y. Takagi and T. Yokoyama. Spin reorientation transitions of Ni/Pd(111) films induced by Fe deposition. *Physical Review B* **81**, 214442 (2010).
- [101] F. Schiller, S. V. Halilov and C. Laubschat. Mn 3d majority spin states in $c(2 \times 2)$ Mn/fcc-X(001) systems (X = Fe, Co, Ni, Cu). *Journal of Physics Condensed Matter* **17**, 3153 (2005).
- [102] K.-M. H. Lenssen, A. E. M. De Veirman and J. J. T. M. Donkers. Inverted spin valves for magnetic heads and sensors. *Journal of Applied Physics* **81**, 4915 (1997).
- [103] D. D. Chambliss, R. J. Wilson and S. Chiang. Nucleation and growth of ultrathin Fe and Au films on Cu(100) studied by scanning tunneling microscopy. *Journal of Vacuum Science Technology A* **10**, 1993 (1992).
- [104] P. Torelli, F. Sirotti and P. Ballone. Surface alloying and mixing at the Mn/Fe(001) interface: Real-time photoelectron spectroscopy and modified embedded atom simulations. *Physical Review B* **68**, 205413 (2003).
- [105] P. Mishra, T. Uchihashi and T. Nakayama. Enhanced spin contrast of epitaxial Mn films on Fe(100) by spin-polarized scanning tunneling microscopy. *Applied Physics Letters* **98**, 123106 (2011).
- [106] P. Bruno. Tight-binding approach to the orbital magnetic moment and magnetocrystalline anisotropy of transition-metal monolayers. *Physical Review B* **39**, 865 (1989).

BIBLIOGRAPHY

- [107] H. L. Meyerheim, R. Popescu, D. Sander, J. Kirschner, O. Robach and S. Ferrer. Layer relaxation and intermixing in Fe/Cu (001) studied by surface x-ray diffraction. *Physical Review B* **71**, 035409 (2005).
- [108] Y. Endoh and Y. Ishikawa. Antiferromagnetism of γ Iron Manganese Alloys. *Journal of the Physical Society of Japan* **30**, 1614 (1971).
- [109] R. Thamankar, S. Bhagwat and F. O. Schumann. Structural and magnetic properties of ultrathin fcc $\text{Fe}_x\text{Mn}_{1-x}$ films on Cu(100). *Physical Review B* **69**, 054411 (2004).
- [110] R. Thamankar, S. Bhagwat and F. O. Schumann. Structural and magnetic instabilities in ultrathin Fe-rich alloy films on Cu(100). *Physical Review B* **69**, 054419 (2004).
- [111] A. Kimura, S. Asanao, T. Kambe, T. Xie, S. Watanabe, M. Taniguchi, S. Qiao, E. Hashimoto, H. Namatame, T. Muro, S. Imada and S. Suga. Electron correlation and magnetic properties of $c(2\times 2)\text{CuMn}/\text{Cu}(001)$ two-dimensional surface alloys. *Physical Review B* **76**, 115416 (2007).
- [112] W. L. O'Brien and B. P. Tonner. Surface-enhanced magnetic moment and ferromagnetic ordering of Mn ultrathin films on fcc Co(001). *Physical Review B* **50**, 2963 (1994).
- [113] H. A. Dürr, G. van der Laan, D. Spanke, F. U. Hillebrecht and N. B. Brookes. Electron-correlation-induced magnetic order of ultrathin Mn films. *Physical Review B* **56**, 8156 (1997).
- [114] J. Dresselhaus, D. Spanke, F. U. Hillebrecht, E. Kisker, G. van der Laan, J. B. Goedkoop and N. B. Brookes. Antiferromagnetic coupling of Mn adsorbates to Fe(100). *Physical Review B* **56**, 5461 (1997).
- [115] P. Gambardella, A. Dallmeyer, K. Maiti, M. C. Malagoli, W. Eberhardt, K. Kern and C. Carbone. Ferromagnetism in one-dimensional monatomic metal chains. *Nature* **416**, 301 (2002).

- [116] P. Gambardella, S. Rusponi, M. Veronese, S. S. Dhesi, C. Grazioli, A. Dallmeyer, I. Cabria, R. Zeller, P. H. Dederichs, K. Kern, C. Carbone and H. Brune. Giant Magnetic Anisotropy of Single Cobalt Atoms and Nanoparticles. *Science* **300**, 1130 (2003).
- [117] S. Imada, A. Yamasaki, S. Suga, T. Shima and K. Takanashi. Perpendicular magnetization of L1₀-ordered FePt films in the thinnest limit. *Applied Physics Letters* **90**, 132507 (2007).
- [118] M. Kitamura, K. Horiba, M. Kobayashi, E. Sakai, M. Minohara, T. Mitsuhashi, A. Fujimori, T. Nagai, H. Fujioka and H. Kumigashira. Spatial distribution of transferred charges across the heterointerface between perovskite transition metal oxides LaNiO₃ and LaMnO₃. *Applied Physics Letters* **108**, 111603 (2016).
- [119] J. P. Perdew, K. Burke and M. Ernzerhof. Generalized Gradient Approximation Made Simple. *Physical Review Letters* **77**, 3865 (1996).
- [120] T. Ozaki. Variationally optimized atomic orbitals for large-scale electronic structures. *Physical Review B* **67**, 155108 (2003).
- [121] A. P. Malozemoff. Random-field model of exchange anisotropy at rough ferromagnetic-antiferromagnetic interfaces. *Physical Review B* **35**, 3679 (1987).
- [122] J. E. Ortega and F. J. Himpsel. Quantum well states as mediators of magnetic coupling in superlattices. *Physical Review Letters* **69**, 844 (1992).
- [123] M. N. Baibich, J. M. Broto, A. Fert, F. Nguyen van Dau, F. Petroff, P. Etienne, G. Creuzet, A. Friederich and J. Chazelas. Giant magnetoresistance of (001)Fe/(001)Cr magnetic superlattices. *Physical Review Letters* **61**, 2472 (1988).
- [124] O. Pietzsch, A. Kubetzka, M. Bode and R. Wiesendanger. Real-Space Observation of Dipolar Antiferromagnetism in Magnetic Nanowires by Spin-Polarized Scanning Tunneling Spectroscopy. *Physical Review Letters* **84**, 5212 (2000).

BIBLIOGRAPHY

- [125] A. Wachowiak, J. Wiebe, M. Bode, O. Pietzsch, M. Morgenstern and R. Wiesendanger. Direct Observation of Internal Spin Structure of Magnetic Vortex Cores. *Science* **298**, 577 (2002).
- [126] A. Kubetzka, M. Bode, O. Pietzsch and R. Wiesendanger. Spin-Polarized Scanning Tunneling Microscopy with Antiferromagnetic Probe Tips. *Physical Review Letters* **88**, 057201 (2002).
- [127] M. Bode, O. Pietzsch, A. Kubetzka and R. Wiesendanger. Shape-Dependent Thermal Switching Behavior of Superparamagnetic Nanoislands. *Physical Review Letters* **92**, 067201 (2004).
- [128] A. Kubetzka, P. Ferriani, M. Bode, S. Heinze, G. Bihlmayer, K. von Bergmann, O. Pietzsch, S. Blügel and R. Wiesendanger. Revealing Antiferromagnetic Order of the Fe Monolayer on W(001): Spin-Polarized Scanning Tunneling Microscopy and First-Principles Calculations. *Physical Review Letters* **94**, 087204 (2005).
- [129] P. Ferriani, K. von Bergmann, E. Y. Vedmedenko, S. Heinze, M. Bode, M. Heide, G. Bihlmayer, S. Blügel and R. Wiesendanger. Atomic-Scale Spin Spiral with a Unique Rotational Sense: Mn Monolayer on W(001). *Physical Review Letters* **101**, 027201 (2008).
- [130] T. Kawagoe, Y. Iguchi, T. Miyamachi, A. Yamasaki and S. Suga. Spiral Terraces and Spin Frustration in Layered Antiferromagnetic Cr (001) Films. *Physical Review Letters* **95**, 207205 (2005).
- [131] M. Bode, M. Heide, K. von Bergmann, P. Ferriani, S. Heinze, G. Bihlmayer, A. Kubetzka, O. Pietzsch, S. Blügel and R. Wiesendanger. Chiral magnetic order at surfaces driven by inversion asymmetry. *Nature* **447**, 190 (2007).
- [132] C. L. Gao, W. Wulfhekel and J. Kirschner. Revealing the 120° Antiferromagnetic Néel Structure in Real Space: One Monolayer Mn on Ag(111). *Physical Review Letters* **101**, 267205 (2008).

- [133] S. Andrieu, M. Finazzi, P. Bauer, H. Fischer, P. Lefevre, A. Traverse, K. Hricovini, G. Krill and M. Piecuch. Growth, structure, and magnetic properties of thin Mn films epitaxially grown on (001) bcc Fe. *Physical Review B* **57**, 1985 (1998).
- [134] C. Grazioli, D. Alfè, S. R. Krishnakumar, S. S. Gupta, M. Veronese, S. Turchini, N. Bonini, A. Dal Corso, D. D. Sarma, S. Baroni and C. Carbone. Spin-Flop Ordering from Frustrated Ferro- and Antiferromagnetic Interactions: A Combined Theoretical and Experimental Study of a Mn/Fe(100) Monolayer. *Physical Review Letters* **95**, 117201 (2005).
- [135] M. Ziegler, N. Ruppelt, N. Néel, J. Kröger and R. Berndt. Control of spin-polarized current in a scanning tunneling microscope by single-atom transfer. *Applied Physics Letters* **96**, 132505 (2010).
- [136] A. Hubert and R. Schäfer. *Magnetic Domains* (Springer-Verlag, Berlin, 1998).
- [137] J. Honolka, T. Y. Lee, K. Kuhnke, A. Enders, R. Skomski, S. Bornemann, S. Mankovsky, J. Minár, J. Staunton, H. Ebert, M. Hessler, K. Fauth, G. Schütz, A. Buchsbaum, M. Schmid, P. Varga and K. Kern. Magnetism of FePt Surface Alloys. *Physical Review Letters* **102**, 067207 (2009).
- [138] U. Schlickum, W. Wulfhekel and J. Kirschner. Spin-polarized scanning tunneling microscope for imaging the in-plane magnetization. *Applied Physics Letters* **83**, 2016 (2003).

Biography

Personal data:

Full name	Shuhei Nakashima
Born	May 26, 1990, Matsudo, Chiba, Japan
Nationality	Japanese

Curriculum Vitae:

- Apr. 2017-Mar. 2018 Research Fellowships for Young Scientists (DC2),
Japan Society for the Promotion of Science (JSPS)
- Apr. 2015-Mar. 2018 Department of Physics, School of Science,
and Institute for Solid State Physics (ISSP),
University of Tokyo
Ph.D student (Supervisor: Prof. Dr. F. Komori)
- Apr. 2013-Mar. 2015 Department of Nanoscience,
Graduate School of Advanced Integration Science,
Chiba University
MS student (Supervisor: Prof. Dr. T. K. Yamada)
- Apr. 2009-Mar. 2013 Department of Nanoscience, Faculty of Engineering,
Chiba University
BS student

Acknowledgements

First of all, I would like to thank **Prof. Dr. Fumio Komori** for giving me the chance to do research in his group, the supervision and the steady support of my work. His deep understanding of physics and great environment with extraordinary instrumental enable me to concentrate to progress this project.

I would like to thank **Dr. Toshio Miyamachi** for his thoughtful advises not only STM techniques but also not only synchrotron radiation experiment. His advises and jokes always encouraged me at any time.

I am grateful to the members of Komori laboratory: **Mr. Takushi Iimori, Mr. Norikazu Kawamura, Dr. Masamichi Yamada, Dr. Koichiro Ienaga, Dr. Yukio Takahashi, Dr. Kota Iwata, Mr. Sogen Toyohisa, Mr. Tadashi Tamura, Mr. Takuma Hattori** and **Mr. Kaishu Kawaguchi** for much supports during my Ph.D work.

I would like to acknowledge the collaborators in the synchrotron center UVSOR: **Prof. Dr. Toshihiko Yokoyama, Dr. Yasumasa Takagi** and **Ms. Madoka Uozumi**.

I wish to thank the theoretical supports provided by **Prof. Dr. Shinji Tsuneyuki, Prof. Dr. Yoshihiro Gohda** and **Dr. Yasutomi Tatetsu**.

I want to thank to **Ms. Natsumi Ishibashi** and **Ms. Michiko Komaki** helping my life in ISSP.

I want to acknowledge the financial support by Iwai Hisao Memorial Tokyo Scholarship Education Foundation and Japan Society for the Promotion of Science (JSPS).

Finally, I would like to express my special thank to my family.